

Peak and residual responses of steel moment-resisting and braced frames under pulse-like near-fault earthquakes

Cheng Fang^{a,b}, Qiuming Zhong^b, Wei Wang^{a,b,*}, Shuling Hu^b, Canxing Qiu^c

^a State Key Laboratory of Disaster Reduction in Civil Engineering, Tongji University, Shanghai 200092, China

^b Department of Structural Engineering, Tongji University, Shanghai 200092, China

^c School of Civil Engineering, Shandong University, Jinan, Shandong 250061, China

ARTICLE INFO

Keywords:

Near-fault earthquakes
Steel moment-resisting frames
Braced frames
Self-centring brace
Buckling-restrained brace (BRB)
Residual inter-storey drift
Seismic resilience

ABSTRACT

This paper presents the behaviour of steel moment resisting and braced frames under pulse-like near-fault earthquakes. The key properties for characterizing near-fault ground motions with forward directivity and fling step effects are discussed, and the influence of varying brace properties on the key engineering demand parameters such as maximum inter-storey drift (MID), residual inter-storey drift (RID) and peak absolute floor acceleration (PA) is revealed. Among other findings, it is shown that the structural responses are related to spectral accelerations, PGV/PGA ratios, and the pulse period of near-fault ground motions. The moment resisting and self-centring braced frames (MRFs and SC-BRBFs) generally have comparable MID levels, while the buckling-restrained braced frames (BRBFs) tend to exhibit lower MIDs. Increasing the post-yield stiffness of the braces decreases the MID response. The SC-BRBFs generally have mean residual drifts less than 0.2% under all the considered ground motions. However, much larger RIDs are induced for the MRFs/BRBFs under the near-fault ground motions, suggesting that these structures may not be economically repairable after the earthquakes. From a non-structural performance point of view, the SC-BRBFs show much higher PA levels compared with the other structures. A good balance among the MID, RID, and PA responses can be achieved when “partial” SC-BRBFs are used. To facilitate performance-based design, RID prediction models are finally proposed which enable an effective evaluation of the relationship between MID and RID.

1. Introduction

Steel moment resisting frames (MRFs) designed in accordance with modern codes are deemed to have satisfactory ductility, energy dissipation capacity, and collapse resistance against strong earthquakes. Steel braced frames are also a prevailing class of lateral load resisting structural system, although conventional steel braces are prone to global and local buckling under compression, which compromises their energy dissipation capability [1]. Alternatively, buckling-restrained braces (BRBs) have plump hysteretic behaviour under cyclic loading, and they have received great attention among seismic researchers and practitioners [2–5]. From a performance-based design point of view, however, the satisfactory seismic performance of both MRFs and buckling-restrained braced frames (BRBFs) are realised at the cost of considerable residual drifts with the damage occurring at major structural members such as beams, connection zones, and braces. An investigation carried out by McCormick et al. [6] suggested that a residual drift exceeding 0.5% after earthquakes may lead to prohibitively

high repair cost for the structure, which, as a result, may have to be demolished. At the meantime, researchers revealed that the average residual drift for MRFs typically exceeds 0.5% and 1.0% under the design-based earthquake (DBE) and maximum considered earthquake (MCE), respectively [7,8], and these values can be even higher for BRBFs [9,10].

The emergence of self-centring buckling-restrained braces (SC-BRBFs) enables improved seismic performance of steel braced frames. Employing posttensioning (PT) technology [11], Christopoulos et al. [12] and Chou et al. [13,14] successfully developed full-scale multi-core SC-BRBFs which show stable flag-shaped hysteretic responses under cyclic loading. Zhou et al. [15] experimentally examined a new type of SC-BRBFs utilising fibre-reinforced polymer composite tendons. The brace specimens were proved to meet the ductility, energy dissipation and self-centring requirements. Another promising material candidate for developing SC-BRBFs is shape memory alloy (SMA) which is a novel class of metals capable of recovering large strains (up to 8–10%) immediately upon unloading [16–18]. It has been shown that SMA

* Corresponding author at: State Key Laboratory of Disaster Reduction in Civil Engineering, Tongji University, Shanghai 200092, China.

E-mail address: weiwang@tongji.edu.cn (W. Wang).

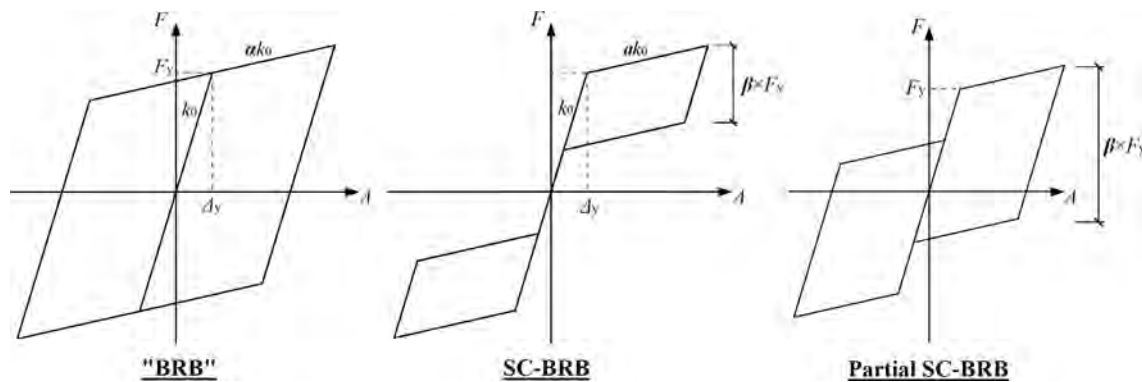


Fig. 1. Simplified hysteretic model of BRB, SC-BRB, and partial SC-BRB.

components can effectively provide self-centring and additional energy dissipation for SC-BRBs [19,20], and some researchers also consider SMA components for self-centring beam-to-column connections [21–25]. At system level, Moradi et al. [26] found that self-centring buckling-restrained braced frames (SC-BRBFs) and BRBFs have comparable maximum inter-storey drift responses, but the residual drift for the former is significantly reduced. Kari et al. [27] revealed that a combined use of both SC-BRBs and normal BRBs in a steel frame could effectively control the maximum drift whilst reducing the residual drift. A similar finding was reported by Eatherton et al. [28], where it was confirmed that structures can have negligible residual drift even if the brace itself exhibits certain ‘static’ residual deformation. Qiu and Zhu [29] warned that a high-mode effect tends to cause concentrated drift in the upper part of SC-BRBFs if the energy dissipation capability is insufficient.

It is clearly seen that a great progress has been made on understanding the fundamental seismic performance of steel MRFs and BRBFs. SC-BRBFs have also been attracting continuous research interests over the past decade. However, the existing studies paid insufficient attention on their behaviour under pulse-like near-fault ground motions, especially from the structural resilience point of view. Near-fault ground motions can be characterized by large, long-period velocity pulses in the fault-normal direction when the fault rupture propagates towards the site, normally with a speed close to the shear wave velocity. In this case, high amount of seismic energy is released in a short time at the ‘forward-directivity’ site, causing much higher demands for engineering structures compared with the case of far-field earthquakes [30,31]. ‘Fling step’, which occurs parallel to strike or dip directions, is another typical near-fault ground motion characteristic that is featured by a unidirectional large-amplitude velocity pulse with a permanent offset of the ground [32]. These characteristics have been recorded in a large number strong earthquakes, including the 1979 Imperial Valley, 1992 Landers, 1994 Northridge, 1995 Kobe, and 1999 Chi-Chi earthquakes, and have attracted significant attention among the community of structural engineers. Research focus has been mainly on the responses of idealised single-degree-of-freedom (SDOF) systems [33,34] and was later extended to more sophisticated structural systems including both fixed-base building frames [30,35–38] and based-isolated systems [39,40]. The behaviour of high-performance structural systems against pulse-like near-fault earthquakes has also been evaluated [41,42].

It has been recognized that pulse-like near-fault earthquakes generally induce larger inelastic deformation demand than far-field ones. In particular, the pulse effect could change the ductility and energy dissipation demands of multi-storey framed buildings, and thus affects the key engineering demand parameters such as maximum inter-storey drift (MID), maximum residual inter-storey drift (RID), and peak absolute floor acceleration (PA). Due to the pulse nature of near-fault ground motions, permanent drift may be more easily accumulated in

structures with a full hysteretic response (e.g. MRFs and BRBFs), and the drift may be further accumulated during aftershocks. Therefore, the RID, which is one of the most important metrics indicating the potential damage level and the associated resilience performance, should be examined in detail. Although there is evidence that SC-BRBFs can effectively reduce RID under a wide range of ground motion types [43], the collapse resistance and serviceability performances (i.e., MID and PA) of these structures under near-fault earthquakes are not well understood. Furthermore, the sensitivity of BRBFs and SC-BRBFs to a number of key brace parameters (e.g., the post-yield stiffness and energy dissipation factor) under near-fault earthquakes is still unclear.

This paper sheds considerable light on the behaviour of steel moment-resisting and braced frame buildings under near-fault earthquakes. The prototype MRFs are three-storey and nine-storey steel office buildings (located in Los Angeles) designed as part of the SAC project [44]. For comparison purposes, the prototype MRFs are redesigned as braced steel frames according to ASCE 7-10 [45], enabling different types of braces with various bracing parameters to be considered. All the structures are designed based on design-compatible response spectrums with no particular consideration for near-fault pulse-like effects. These structures are then assessed in terms of MID, RID, and PA responses by using a suite of near-fault ground motion records, covering both forward directivity and fling step effects. This is followed by a detailed discussion on the influence of the varying brace parameters on the structural performance, and the observed trends are subsequently used for the proposal of practical RID prediction models.

2. Basic characteristics of SC-BRBs and BRBs

SC-BRBs, which can be achieved by either the PT or SMA technique, typically exhibit flag-shaped hysteretic behaviour. For an idealised flag-shaped curve as shown in Fig. 1, the axial load-deformation response first follows a linear path and then achieves a ‘yielding’ point before advancing into the ‘post-yield’ stage. Upon unloading, the load first decreases linearly and then enters into the unloading plateau and finally decreases to zero ideally with no residual displacement. It is noted that the ‘yielding’ point is not caused by material yielding, but is instead triggered by decompression of the PT elements or by martensitic transformation of the SMA components. The energy dissipation, i.e., the area enveloped by the flag-shaped hysteresis, is contributed by extra energy dissipative devices (for the PT solution) or by inherent material damping (for the SMA solution).

The force-deformation relationship of a flag-shaped model is characterized by four key parameters, namely, initial stiffness k_0 , yield strength F_y , post-yield stiffness ratio α , and energy dissipation factor β . In particular, the post-yield stiffness ratio (α) may vary significantly with different considered self-centring techniques. For instance, SMA components normally exhibit a pronounced post-yield stiffness (i.e., a large value of α) due to forward transformation slope and martensitic

hardening [46]. The energy dissipation factor (β) describes the shape of the hysteretic loop, where $\beta = 0.0$ indicates an elastic bilinear system with no energy dissipation, and $\beta = 2.0$ makes an idealised elastoplastic behaviour with full hysteresis. When β ranges between 1.0 and 2.0, a “pinching-like” behaviour is exhibited in the hysteretic loop, and certain residual deformation occurs upon static unloading. This behaviour is also called partial self-centring. In practical design, the value of β may be tuned in order to achieve a proper balance between energy dissipation and self-centring capability, both are related to the peak and residual responses of the structures, as discussed later.

On the other hand, a BRB is a structural member that exhibits a ductile load-deformation behaviour under both tension and compression with full hysteresis. The cyclic behaviour of a BRB is sufficiently represented in practice by an inelastic hysteretic model that considers a uniaxial Giuffre-Menegotto-Pinto material behaviour (i.e., “sophisticated” BRB model) [47]. Alternatively, considering $\beta = 2.0$ in a flag-shaped model leads to an idealised bilinear presentation of the BRB behaviour (i.e., “idealised” BRB model), and such simplification for BRBs has also been adopted by researchers for system-level analysis [27,29]. In the current study, the idealised BRB presentation is considered. The simplification enables a systematic comparison between SC-BRBs and BRBs with comparable parameters, and as a result the mechanism that attributes to the difference in the system-level structural behaviour can be effectively revealed.

3. Prototype buildings

3.1. Design and modelling of MRFs

The three-storey and nine-storey steel buildings designed for the SAC steel project [44] are selected as the prototypes MRFs. The structures were originally designed as office buildings located on a stiff soil site (Site Class D) in Los Angeles. The lateral load resisting system in both directions consists of two special MRFs on the perimeter of the building. This study focuses on the 2D frames that represent half of the structures in the north-south (NS) direction. As illustrated in Fig. 2(a), the three-storey building has four bays in the NS direction, including three MRF bays and one bay for resisting gravity load only. Fixed column feet are considered for the building. The nine-storey building includes a basement level in addition to nine stories above the ground level. The building has five bays of MRF in the NS direction, although one external connection is designed as pinned to avoid bi-axial bending in the corner column. For both buildings, the design yield strengths of the beams and columns are 248 MPa and 345 MPa, respectively. The buildings are required to conform to a drift limit of $h/400$ (h = storey height) under normal design load combinations. More structural design details for the MRFs can be found elsewhere [44].

The prototype MRF buildings are modelled using the nonlinear dynamic analysis program OpenSees [48]. Basic centreline models of the MRFs are built. The beam and column members are simulated via nonlinear force-based beam-column elements with fibre sections, such that the development and distribution of plasticity along the length and depth of the members are included. Each fibre is modelled using Steel01 material with a post-yielding stiffness ratio of 0.03 [44]. Rigid connections are assumed for the MRF bays, and pinned connections are used where necessary, according to the design. The seismic mass is taken as half the total structural mass, where the weight from the tributary area is directly applied to the 2D frame, while the remaining weight is applied to adjacent lean columns such that the P- Δ effect is fully considered. Such model enables a conservative prediction of structural deformation responses as the contributions to sustaining lateral load/P- Δ effect from the gravity frame and infill walls are ignored. The structural model assumes Rayleigh damping with a 2% damping ratio for the first and second modes of vibration. The first mode periods of the three- and nine-storey MRF building models are 1.01 s and 2.27 s, respectively.

3.2. Design and modelling of BRBFs

Both the three- and nine-storey MRFs are redesigned as BRBFs for comparison purpose. The BRBFs are assumed to locate at the same site as the MRFs. A reduced-strength version of the bare steel frame was first designed to satisfy the basic gravity load resistance requirement. Inverted-V BRBs were then added to provide significant seismic load resistance, and these members are mainly responsible for storey drift control. The BRBFs are designed as dual systems where the bare steel frame (with rigid beam-to-column connections) contributes to the overall lateral resistance. It should be kept in mind that pin connections enabling a reduced cost are also allowed and are quite popular for BRBFs in the current practice, but for self-centring structural systems, a certain level of redundancy is still desired. In view of this, dual systems were adopted for the current BRBFs to enable a direct comparison against the SC-BRBs.

A trail design was performed according to ASCE 7-10 [45] for the three- and nine-storey BRBFs by using the equivalent lateral force procedure and the modal response spectrum analysis, respectively. The following design response spectral values were assigned to the site: $S_{DS} = 2/3S_{MS} = 1.376$ g and $S_{D1} = 2/3S_{M1} = 0.707$ g. The BRBFs were considered as Risk Category II buildings with an importance factor of $I_e = 1.0$. As the steel frame also contributes to lateral load resistance, the response modification coefficient (R) and the deflection amplification factor (C_d) were taken as 8.0 and 5.0, respectively, according to the ASCE 7-10 requirement. The allowable storey drifts are 2.0% under the DBE level, and the structural members were modified as necessary to meet the storey drift limit.

The final selected beam and column sections and the properties of the braces for the three- and nine-storey BRBFs are illustrated in Fig. 2(b). The post-yield stiffness ratios (α) for all the BRBs are set as 0.05. Based on the equivalent lateral force procedure or the modal response spectrum analysis method, and considering $C_d = 5.0$, the estimated maximum storey drifts of the three- and nine-storey BRBFs are 1.60% and 1.45% respectively, which satisfy the drift limit of 2.0% under the DBE level. Similar to the MRFs, basic centreline models for the BRBFs were built in OpenSees. The BRB elements were modelled using Truss elements that resist axial forces only. The material behaviour for the BRB is represented using a Steel01 material, which is a bilinear elastoplastic model with kinematic strain hardening. The first mode periods of the three- and nine-storey BRBFs are 0.64 s and 1.73 s, respectively. As mentioned before, the idealised BRB presentation is used to facilitate direct comparisons with flag-shaped SC-BRB presentations, where the two cases only differ in β . Caution should be exercised that the behaviour of the structures with idealized bilinear braces can be different from the “actual results” where more sophisticated BRB models are employed, and this should be kept in mind when examining the numerical results. The pushover responses of the BRBFs, together with that of the MRFs, are shown in Fig. 3.

Nonlinear time-history analyses were further carried out for the BRBFs. The considered earthquake records, as summarised in Table 1, were selected and scaled based on FEMA P695 for stiff soil site (Site Class D) conditions with a 10% probability of exceedance in 50 years [49]. These are far-field ground motions that exhibit minimal near-fault pulse-like effects. The ground motions were further scaled by 1.5 to represent the maximum considered earthquake (MCE) level. The individual and mean response spectra of the considered far-field earthquake records are shown in Fig. 4(a) together with the design response spectrum.

According to ASCE 7-10, the allowable storey drift obtained from nonlinear time-history analysis can be increased by 25% for Risk Category II buildings. Therefore, the limit of the maximum storey drift is relaxed to 2.5% under the DBE level. For the MCE level, the allowable storey drift may be taken as 3.75% (i.e., $1.5 \times 2.5\%$). According to the nonlinear time-history analysis results, the three-storey BRBF exhibits a mean maximum storey drift of 1.72% and 2.24% under the DBE and

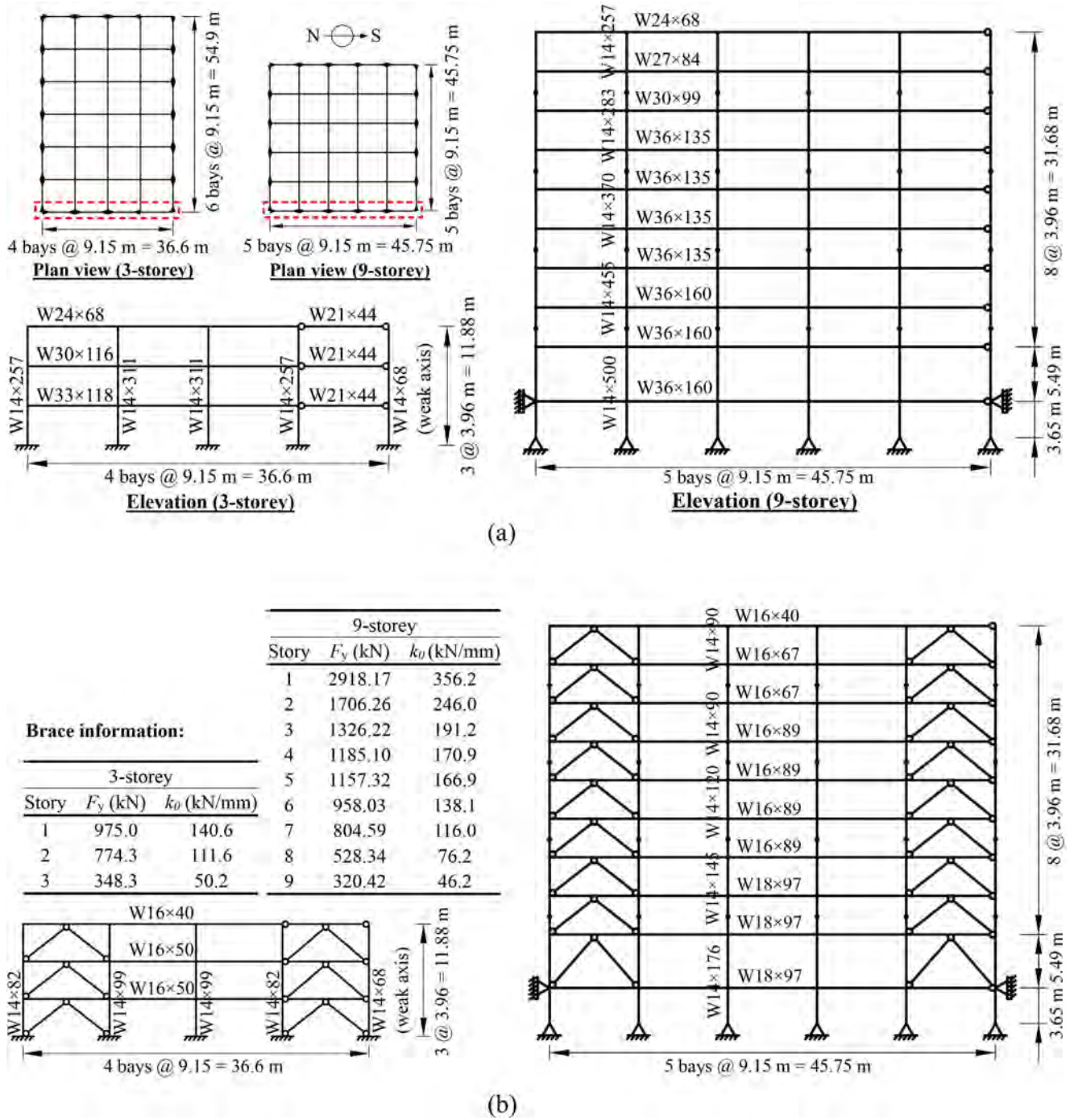


Fig. 2. Layout of prototype buildings: (a) details of MRFs, (b) details of braced frames.

MCE, respectively, and for the nine-storey BRBF, the corresponding values are 1.47% and 2.07%, respectively. Clearly, the buildings satisfy the drift requirements under both DBE and MCE levels.

3.3. Design and modelling of SC-BRBFs

It is assumed that the SC-BRBFs and BRBFs have the same member sizes and they only differ in the energy dissipation factor β of the braces. This makes identical first mode period and lateral stiffness of the two types of structures. For the prototype SC-BRBFs, the brace members have the same initial/post-yield stiffness and yield strength as the BRBs, while a reference case of $\beta = 1.0$ was considered, i.e., half of the energy dissipation of the BRBs. The SC-BRBFs were modelled in

OpenSees using Truss elements with a ‘SelfCentering’ material that simulates the flag-shaped hysteresis of the braces. Since there is no codified static design procedure for self-centring systems, e.g., the response modification coefficient (R) and the deflection amplification factor (C_d) are not available, a nonlinear time-history analysis procedure was directly adopted to examine the storey drift responses of the structures. Employing the same suite of far-field ground motions used for the BRBFs, the mean maximum storey drifts for the three-storey SC-BRBF under the DBE and MCE are 2.04% and 2.91%, respectively; for the nine-storey SC-BRBF, the corresponding values are 1.74% and 2.43%, respectively. Again, the buildings satisfy the drift requirements under both the DBE and MCE according to ASCE 7-10, although the peak drift responses are larger than the BRBFs, which may be attributed

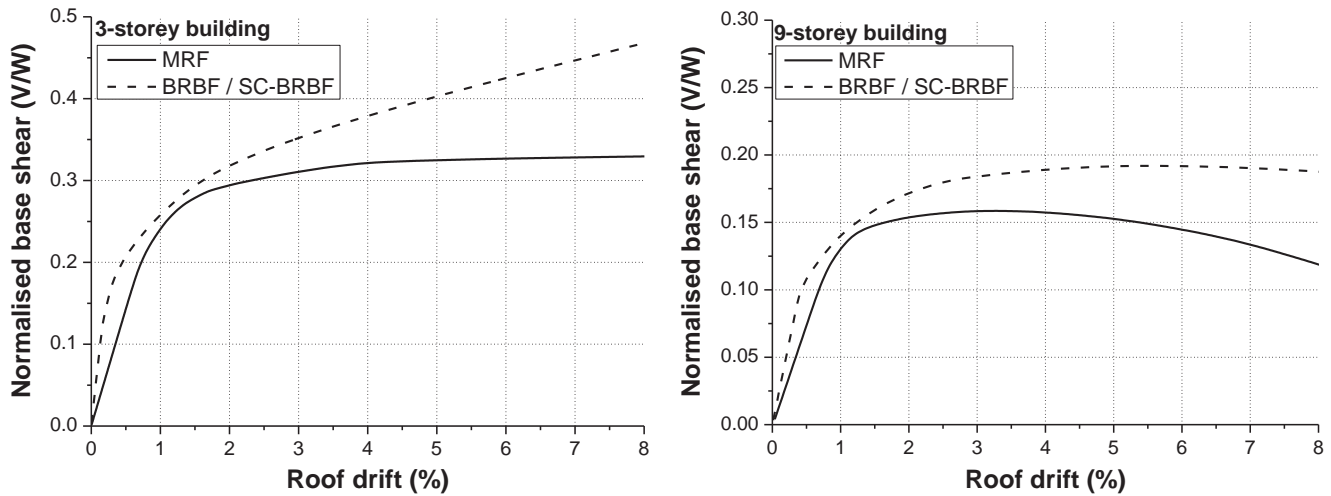


Fig. 3. Pushover responses of steel frames (V = base shear, W = seismic weight).

to the decreased energy dissipation of the SC-BRBFs.

4. Response to near-fault earthquakes

4.1. Selected near-fault ground motions

Having shown that the reference MRFs, BRBFs, and SC-BRBFs satisfy the basic design requirements, their behaviour under near-fault ground motions is investigated herein. A set of 15 near-fault ground motion records, 10 with forward directivity (including 7 historical recordings and the remaining 3 from physical simulations of fault rupture and seismic wave propagation) and 5 with fling step (all historical recordings), were used for the analysis. These ground motions were selected from the Phase-II SAC Steel Project and PEER (Pacific Earthquake Engineering Research Centre) database, and were taken from 8 events in different countries and regions. They are recorded on stiff soil within a distance of 15 km from the rupture fault [50], and the event magnitudes M_w ranges from 6.7 to 7.6. The basic information on the ground motions is summarised in Table 2, and the 5% damped acceleration spectra are shown in Fig. 4(b). In addition, Fig. 5 illustrates the ground acceleration (a_g), velocity (v_g) and displacement (u_g) time-histories of typical selected near-fault ground motions exhibiting forward-directivity or fling step. It is seen that forward-directivity produces ground motions that have large velocity amplitudes with two or multi sided velocity pulses but with unremarkable permanent ground displacement.

Table 1
Basic information on selected far-field ground motions.

Event No.	Earthquake name	Year	Station	Soil type	Magnitude (M_w)	PGA (g)	PGV (cm/s)	PGV/PGA	Scale factor	
									DBE	MCE
FF1	San Fernando	1971	LA-Hollywood Stor	Stiff soil	6.6	0.547	49.19	0.092	2.61	3.91
FF2	Imperial Valley	1979	Delta	Stiff soil	6.5	0.697	76.11	0.111	2.93	4.40
FF3	Imperial Valley	1979	Delta	Stiff soil	6.5	0.607	57.03	0.096	1.73	2.59
FF4	Imperial Valley	1979	El Centro Array #11	Stiff soil	6.5	0.318	30.03	0.096	0.87	1.31
FF5	Imperial Valley	1979	El Centro Array #11	Stiff soil	6.5	0.552	61.27	0.113	1.46	2.18
FF6	Superstition Hills	1987	El Centro Imp. Co.	Stiff soil	6.5	0.650	84.08	0.132	1.82	2.72
FF7	Superstition Hills	1987	El Centro Imp. Co.	Stiff soil	6.5	0.643	101.58	0.161	2.49	3.73
FF8	Superstition Hills	1987	Poe Road (temp)	Stiff soil	6.5	0.895	71.50	0.082	2.00	3.01
FF9	Superstition Hills	1987	Poe Road (temp)	Stiff soil	6.5	1.003	109.36	0.111	3.34	5.01
FF10	Loma Prieta	1989	Capitola	Stiff soil	6.9	0.646	42.73	0.068	1.22	1.83
FF11	Loma Prieta	1989	Gilroy Array #3	Stiff soil	6.9	0.406	26.08	0.066	0.73	1.10
FF12	Landers	1992	Coolwater	Stiff soil	7.3	0.652	63.38	0.099	2.30	3.45
FF13	Northridge	1994	Beverly Hills-Mulhol	Stiff soil	6.7	0.961	136.07	0.145	2.31	3.47
FF14	Kocaeli-Turkey	1999	Duzce	Stiff soil	7.5	0.519	67.23	0.132	1.45	2.18
FF15	Duzce-Turkey	1999	Bolu	Stiff soil	7.1	0.594	46.04	0.079	0.82	1.22

The pulse-like nature is best observed in the velocity time history. On the other hand, fling step typically produces a permanent ground offset with a corresponding one-sided dominated velocity pulse, as can be seen from the velocity and displacement time histories. It is noted that both effects can be hardly identified from the acceleration time history alone.

The key properties for characterizing near-fault ground motions include the peak ground acceleration (PGA), peak ground velocity (PGV), PGV/PGA ratio, and pulse period (T_p). These quantities are also given in Table 2. In particular, previous studies showed that the significance of pulsing characteristic increases with the PGV/PGA ratio, where a value exceeding 0.2 typically indicates strong pulse-like ground motions [51]. Pulse period (T_p) is another essential characteristic. Several approaches are practically available to determine T_p , although consensus has not been fully reached so far among seismic engineers. The most convenient yet specific approach is to identify the pulse period by finding the global peak of the velocity response spectrum of the ground motion [52], and such result is often called equivalent pulse period (T_{p-v}). Alternatively, pulse period (T_p) can be estimated based on the zero-crossing time of the velocity pulse in a velocity time history [50], as demonstrated in Fig. 5. Certain subjectivity can be involved when using the latter procedure, especially for complex records with overlapping velocity pulses. For ground motions with a distinguishable single pulse, the two approaches generally lead to similar results. Rodriguez-Marek [53] found that the mean ratio of zero-crossing to

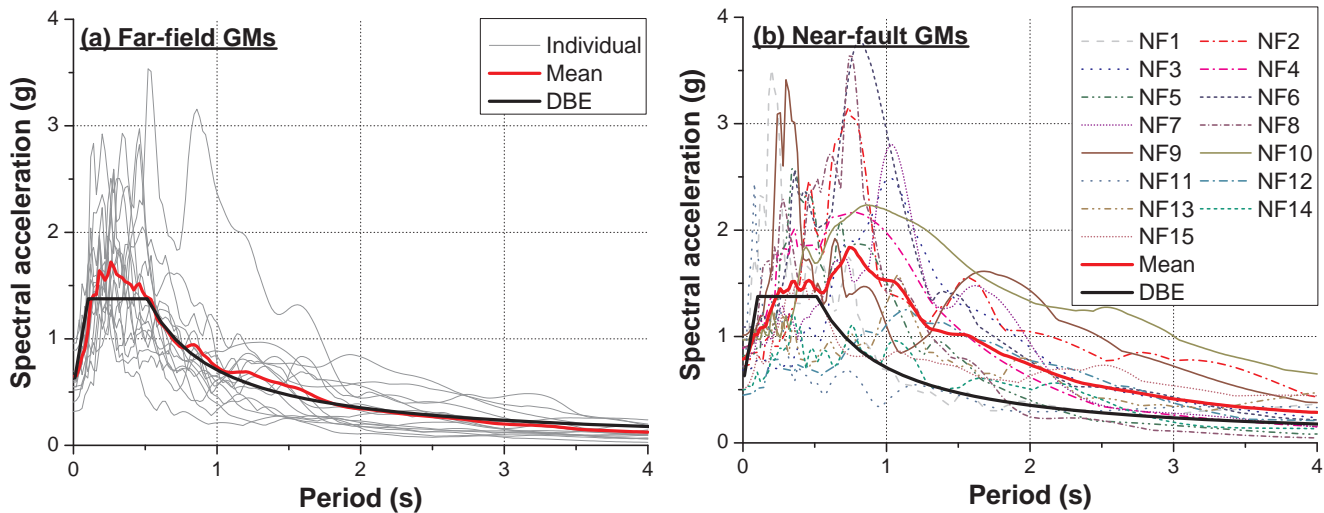


Fig. 4. Elastic response spectra of the selected ground motion (GM) records.

velocity response spectrum results is 0.84 with a standard deviation of 0.28. The pulse periods based on both approaches for the considered ground motions are given in Table 2. It is seen that T_p and T_{p-v} for the selected ground motions range from 0.84 s to 13.87 s and from 0.90 s to 9.32 s, based on the zero-crossing and velocity response spectrum methods, respectively. In addition, a characteristic length-scale measurement, $L_p = a_p T_p^2$, which reflects the persistence of the most energetic pulse to generate inelastic deformations of structures [33,35], is also given in Table 2. Assuming that the velocity pulse can be expressed by a simplified Mavroeidis-Papageorgiou (MP) model [54], the acceleration amplitude (a_p) can be taken as $a_p = 2\pi v_p / T_p$, where v_p is, strictly speaking, the velocity amplitude of the idealised MP pulse but may be considered to be equal to the PGV for the purpose of trend revealing.

Another important issue related to near-fault ground motions is scaling. In contrary to far-field ground motions where spectral amplitudes are scaled monotonically at all periods, the pulse period of near fault ground motions is particularly related to source parameters such as the rise time and fault dimensions, which generally change with magnitude. Therefore, the key inherent properties of near fault ground motions cannot be sufficiently reflected by simple uniform scaling, because the shape of the intermediate- and long-period part of the response changes as the magnitude increases [55]. In light of this, it was decided not to scale the selected near-fault ground motions, such that “true” pulsing characteristics can be reflected. It is observed in Fig. 4(b) that the mean acceleration response spectrum of the selected suite of

near-fault ground motions is not less than the design response spectrum (DBE level) for periods ranging from 0.2T to 1.5T (where T is the fundamental natural period of the structure being considered), and therefore the ASCE 7-10 requirement of seismic response history procedures at DBE level is satisfied. The response spectrum also demonstrates that near-fault records can impose larger demands at longer periods, which is a typical characteristic of pulse-like ground motions.

4.2. Case study

The typical structural response to the considered near-fault ground motions is first illustrated via a case study. The three- and nine-storey structures undergoing the Loma Prieta ground motion and at a distance of 6.3 km from the rupture fault (Lex. Dam station) are selected. The roof drift time-history responses of the structures are shown in Fig. 6(a). The three types of structures generally exhibit a similar level of peak roof drift which occurs at 4.5–5 s, a moment which coincides with the occurrence of the dominant ground velocity pulse, as shown in Fig. 5. Immediately after experiencing the peak roof drift, the structures bounce back with a reversed peak roof drift which is smaller than the previous one. It can be seen that the SC-BRBFs typically experience larger amplitudes of fluctuation after undergoing the peak roof drift, which is attributed to the unique flag-shaped responses of the SC-BRBFs with reduced energy dissipation (compared with BRBs). Nevertheless, the SC-BRBFs tend to oscillate near the zero drift line and finally

Table 2

Basic information on selected near-fault ground motions.

Event No.	Earthquake	Year	Station	Soil type	Magnitude	Distance (km)	PGA (g)	PGV (cm/s)	PGV/PGA	Type	T_p (s)	T_{p-v} (s)	L_p (m)
NF1	Tabas	1978	Tabas	Stiff soil	7.4	1.20	0.978	105.81	0.110	FD	5.24	4.70	34.8
NF2	Loma Prieta	1989	Los Gatos	Stiff soil	7.0	3.50	0.718	172.84	0.246	FD	2.28	3.26	24.7
NF3	Loma Prieta	1989	Lex. Dam	Stiff soil	7.0	6.30	0.687	178.66	0.266	FD	1.56	1.08	17.5
NF4	Northridge	1994	Rinaldi	Stiff soil	6.7	7.50	0.891	174.22	0.200	FD	1.39	1.06	15.2
NF5	Kobe	1995	KJMA	Stiff soil	6.9	0.96	0.821	81.22	0.101	FD	0.84	0.90	4.3
NF6	Kobe	1995	Kobe	Stiff soil	6.9	3.40	1.089	160.17	0.150	FD	2.16	0.88	21.7
NF7	Kobe	1995	Takatori	Stiff soil	6.9	4.30	0.787	144.73	0.188	FD	1.78	1.28	16.2
NF8	Elysian Park 2	–	–	Stiff soil	7.1	10.70	0.904	96.81	0.109	FD	0.84	0.76	5.1
NF9	Elysian Park 3	–	–	Stiff soil	7.1	11.20	1.014	155.07	0.156	FD	2.64	1.92	25.7
NF10	Palos Verdes 2	–	–	Stiff soil	7.1	1.50	0.969	287.86	0.303	FD	3.28	2.60	59.3
NF11	Landers	1992	Landers	Stiff soil	7.3	1.10	0.714	136.05	0.194	FS	5.70	4.16	48.7
NF12	Chi Chi	1999	TCU52	Stiff soil	7.6	1.84	0.448	220.67	0.503	FS	13.87	9.80	192.2
NF13	Chi Chi	1999	TCU65	Stiff soil	7.6	2.49	0.790	132.48	0.171	FS	6.20	4.68	51.6
NF14	Chi Chi	1999	TCU67	Stiff soil	7.6	1.11	0.499	97.47	0.199	FS	3.93	2.28	24.1
NF15	Chi Chi	1999	TCU68	Stiff soil	7.6	3.01	0.512	280.28	0.559	FS	12.15	9.32	213.9

FD = forward directivity, FS = fling step.

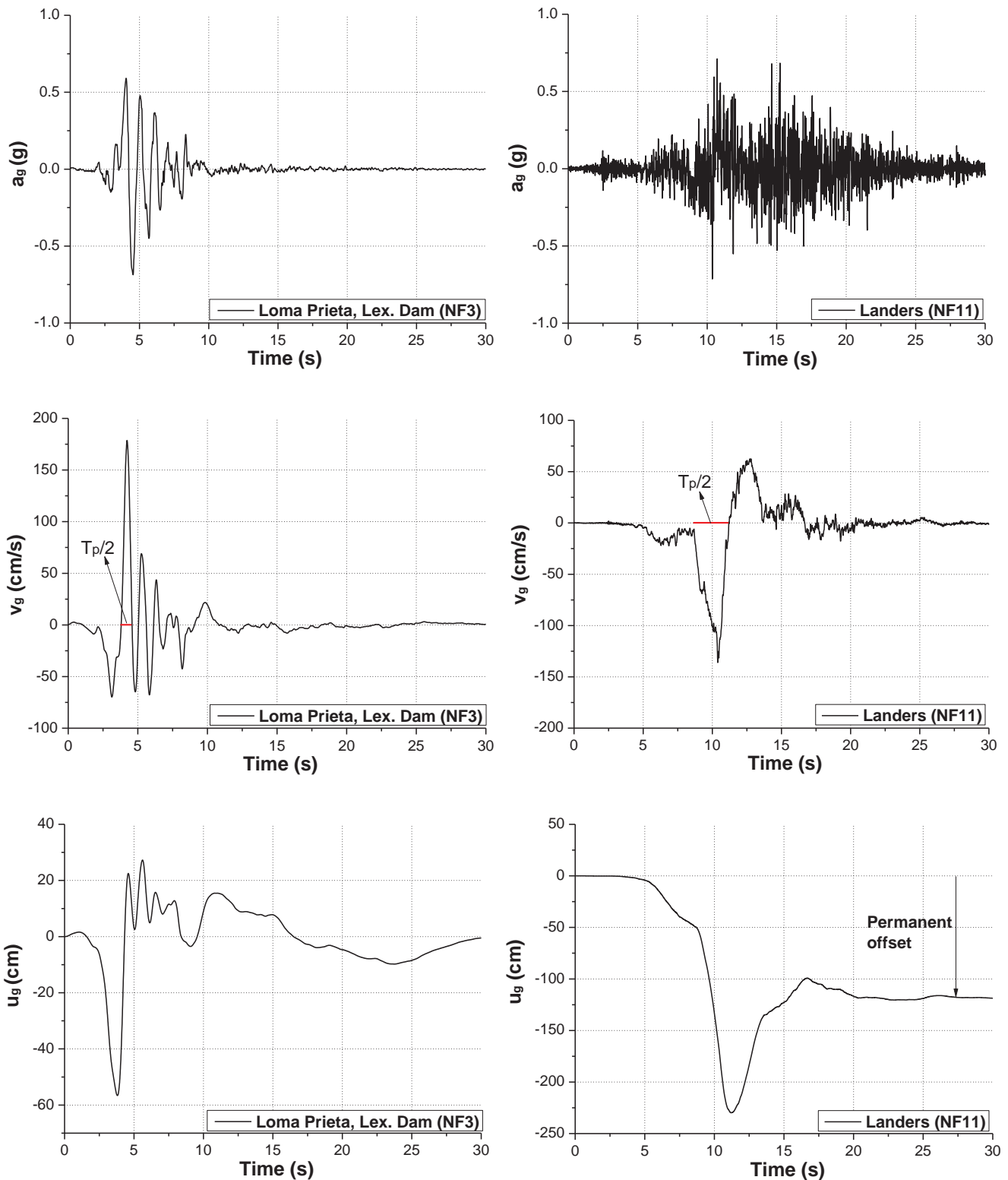


Fig. 5. Typical ground acceleration, velocity, and displacement time-histories of selected near-fault ground motions.

negligible residual deformation occurs during the attenuation of vibration, whereas the MRFs and BRBFs oscillate with certain excursions of roof drift, which is a major cause of their final residual deformation. The roof drift response indicates that the braces with an increased self-centring tendency but reduced energy dissipation (i.e., SC-BRB) do not necessarily enlarge the peak drift response. It is also implied that for the near-fault ground motions, the peak drift response is mainly caused by

the predominant ground velocity pulse. For the ground motion particularly considered in the case study, the peak roof drifts of the three- and nine-storey structures are on the order of 4–6% and 2.5–3%, respectively. The corresponding residual roof drifts for the MRFs/BRBFs are on the order of 0.5–1.5%, but the SC-BRBFs exhibit almost no residual roof drift.

Fig. 6(b) shows the detailed axial force-deformation responses of the

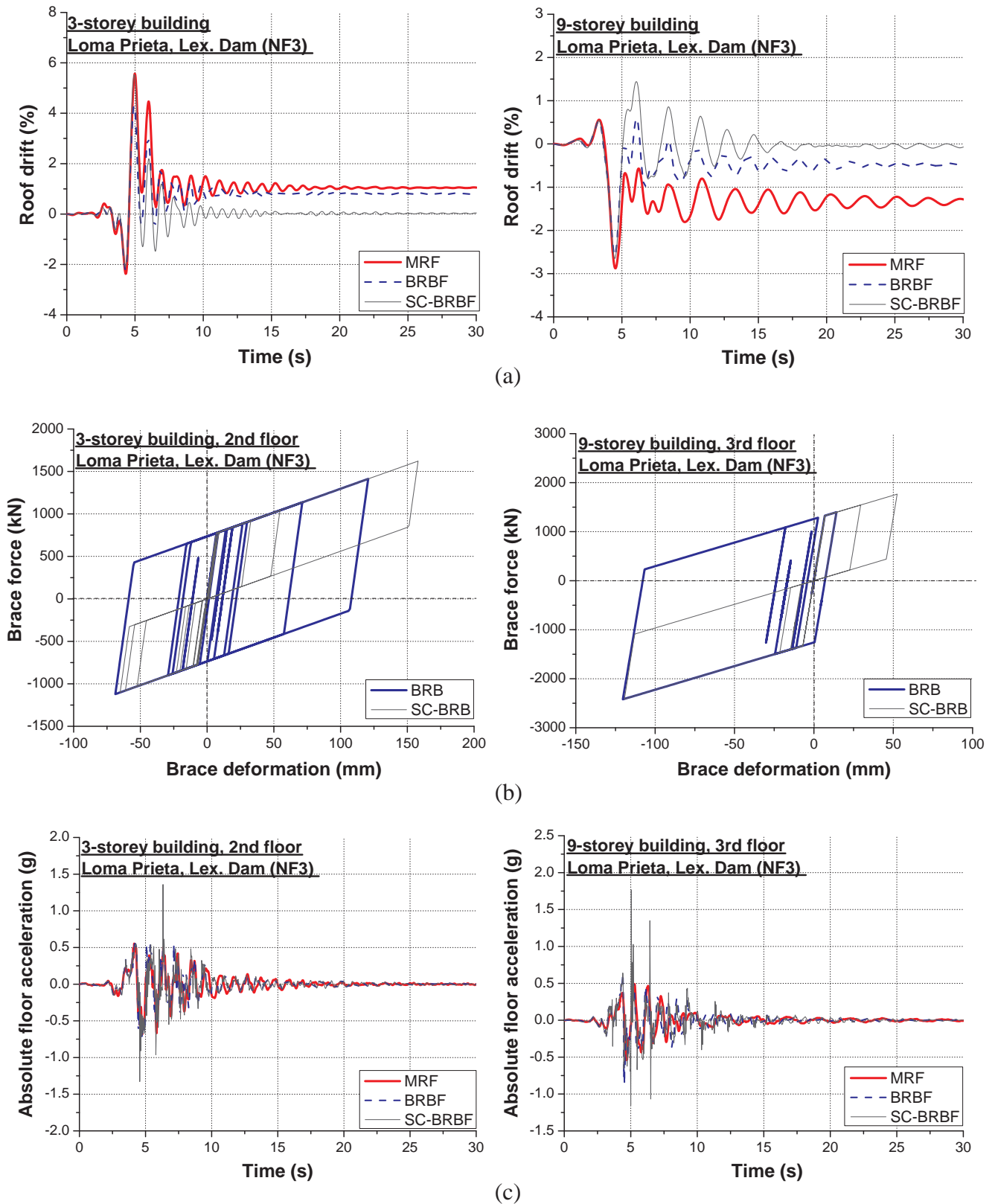


Fig. 6. Case study: (a) roof drift time histories, (b) behaviour of braces, (c) acceleration response.

BRBs and SC-BRBs at selected floor levels. The ability of the SC-BRBs to provide self-centring and moderate energy dissipation, in contrast to the full hysteretic response of the BRBs, is clearly shown in the figure. It should be noted that the braces in this study are assumed to have sufficient deformability without failure. Being in line with the drift

response, the SC-BRBs are shown to have comparable or slightly larger peak axial displacement but significantly smaller residual displacement than the BRBs. For both the three- and nine-storey structures, the maximum axial deformation demand of the considered braces is on the order of 150 mm. It is recalled that the typical length of each brace is

6.05 m, and an axial displacement of 150 mm corresponds to a relative member elongation or compression of at least 2.5%. Such a high deformation demand may make the PT solution impractical, noting that the total elastic strain (including that for prestress) for high-strength PT bars is typically less than 0.5%. The result warns that a very high deformation demand is expected for structures under near-fault pulse-like earthquakes. Improved multi-core PT-based SC-BRBs, or SMA-based solutions, may have to be adopted to provide adequate brace deformability [13–15].

Fig. 6(c) shows the absolute floor acceleration time-history responses of the considered structures. The SC-BRBFs show larger floor acceleration responses than the MRFs and BRBFs. Taking the 2nd floor of the three-storey SC-BRBF for example, the peak floor acceleration value achieves nearly 1.4 g, which is twice the PGA. This means that the ground acceleration is significantly amplified by the SC-BRBs, and as a result significant economic losses related to the damage to non-structural components and systems can be induced. A similar finding was also reported by Tremblay et al. [43] for the case of far-field earthquakes. The overall trends of floor acceleration response are further discussed in the following section.

4.3. Overall response to near-fault earthquakes

Having illustrated the typical responses of the three types of structures to a specific near-fault earthquake record, an overall view of the behaviour of these structures is presented. Fig. 7 shows the MID, RID, and PA responses of the considered MRFs, BRBFs, and SC-BRBFs to the 15 near-fault ground motions, together with the mean responses to the aforementioned DBE- and MCE-level ground motions that exhibit minimal pulse-like effects.

The MRFs and SC-BRBFs have comparable MID responses under the DBE and MCE, although the former typically has less energy dissipation than the latter. This is because the required energy absorption by a flag-shaped system tends to be less than the comparable system with a fuller hysteresis [56,57]. In addition, the inelastic deformation is not accumulated in the SC-BRBFs, and the oscillation always occurs around the initial position. The BRBFs, especially the three-storey one, exhibit decreased MID responses than the other two structural types under both the far-field and near-fault earthquakes. This could benefit from the high energy dissipation capability as well as the high initial stiffness (compared with the MRFs) of the BRBs. For all the considered steel frames, the near-fault earthquakes lead to significantly larger deformation demands than the DBE and MCE. The mean MID exceeds (or close to) 3.75% for both the MRFs and SC-BRBFs under the near-fault ground motions. It is noticed that due to the high-mode effect, the nine-storey SC-BRBF shows larger peak storey drifts than its MRF and BRBF counterparts at higher floor levels. The finding is consistent with the results reported by Qiu and Zhu [29] who concluded that the high-mode contribution is highly coupled with the fundamental mode of self-centring structures and therefore induces a concentration of enlarged storey drift at top stories. It was also claimed in the literature that the high-mode effect can be effectively mitigated by increasing either the energy dissipation or the post-yield stiffness ratio of the SC-BRBs. Generally speaking, it is demonstrated that hysteretic energy dissipation may not consistently correlate with seismic performance, especially for the new class of self-centring structural systems [58]; however, an optimised response may be achieved with at least a minimum level of energy dissipation capacity together with appropriate α and β values of the SC-BRBs

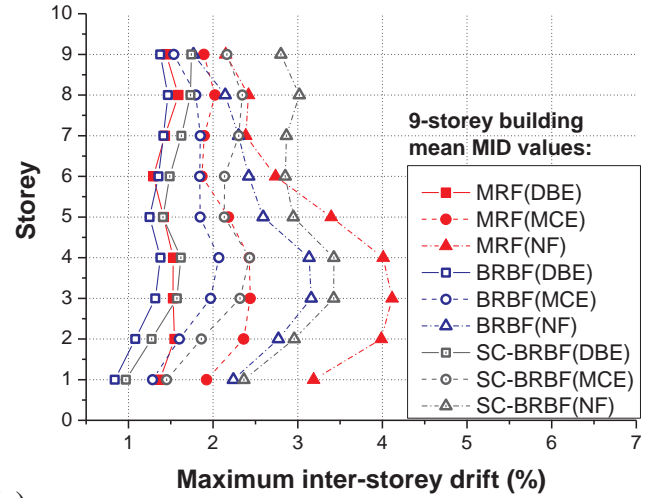
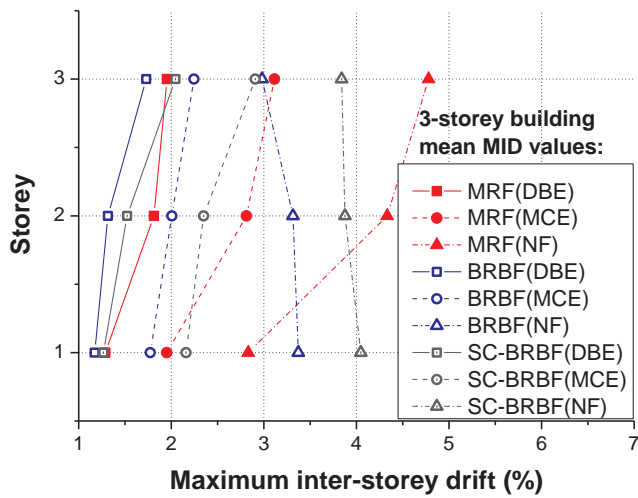
For the RID response, the three- and nine-storey SC-BRBFs have mean residual drifts less than 0.2% under all the considered ground motion records, where the near-fault ground motions lead to slightly larger RID values which are associated with larger MIDs. It should be noted that the minor residual drifts of the SC-BRBFs are mainly from the inelastic deformations of the main frame members rather than from the SC-BRBs. For the MRFs and BRBFs, the mean RID is below 0.3% and

0.5% under the DBE and MCE, respectively. The near-fault ground motions, however, lead to significantly increased RID responses.

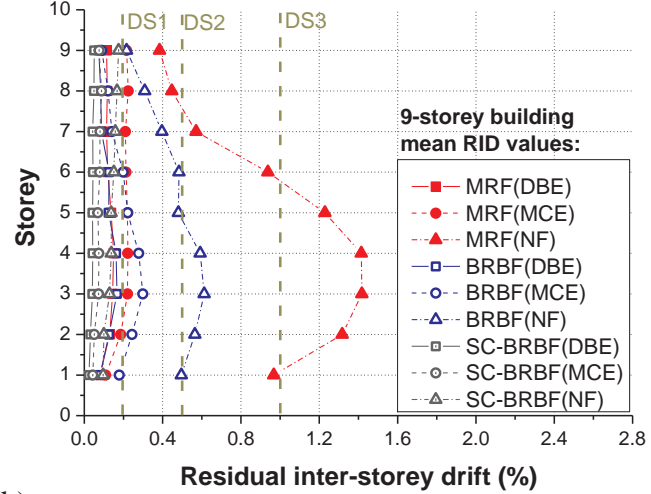
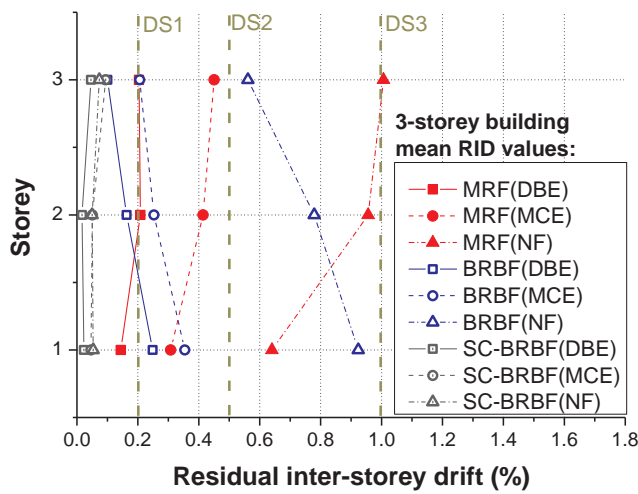
In FEMA P-58 [59], RID limits with four classes are stipulated. The first class, DS1, requires that the RID is less than 0.2% such that 'no structural realignment is necessary for structural stability, but the building may require adjustment and repairs to non-structural and mechanical components'. A relaxed class of DS2 requires the RID to be less than 0.5% such that realignment of structural frame and related structural repairs are economically feasible, and degradation in structural stability is limited. Class DS3 with RID exceeding 0.5% indicates that major structural realignment, which may not be economically and practically feasible, is required to restore margin of safety for lateral stability, and class DS4 with RID exceeding 1.0% means that residual drift is too large that the structure is in danger of collapse from after-shocks. Based on the codified definition, it can be seen from Fig. 7(b) that the SC-BRBFs well satisfy class DS1 under the considered ground motions including the near-fault ones. For the MRFs and BRBFs under the DBE, class DS1 is also satisfied (or slightly exceeded), suggesting that limited repair work is required for these structures. The MCE leads to increased RIDs for the MRFs and BRBFs, although class DS2 is still satisfied. The DBE and MCE responses show that the conventional steel frames, even in the absence of any self-centring technology, may be economically repairable after strong earthquakes. This is, however, not the case when near-fault ground motions are considered. It is seen that the mean RID could exceed the DS3 limit, suggesting that the MRFs and BRBFs are not economically repairable under the near-fault earthquakes. In this context, the critical role played by the SC-BRBs in reducing the RID is clearly demonstrated.

Peak absolute floor acceleration (PA) is another key factor affecting the non-structural building responses including the condition of the contents [60]. Past earthquakes reveal that injuries, fatalities, repair costs and disruption time related to failure of non-structural components far exceeded those associated with structural damages [61]. As can be seen in Fig. 7(c), the SC-BRBFs show much larger PA responses compared with the MRFs and BRBFs under all the considered ground motions, and the difference due to varying structural types is more evident in the lower half of the structures. This implies that a fuller hysteresis via material yielding is more effective in controlling the accelerations "transmitted" into the structures. The above phenomenon has also been reported by Tremblay et al. [43], and it was believed that the increased PA is due to the more abrupt transition points of the flag-shaped hysteresis compared with its elasto-plastic counterpart. More specifically, two adjacent floors have inconsistent storey shear forces during earthquakes and normally the shear force response at one floor lags behind that of the other floor. The abrupt transitions of the flag-shaped braces during the unloading and reloading path leads to larger differences of the shear force between the adjacent stories, which can produce a very short duration, high amplitude floor acceleration pulse. Such an acceleration pulse is less likely to occur in MRFs and BRBFs which have less abrupt transition points during the loading and unloading hysteretic paths. The results also show that the PA response is not necessarily enlarged by pulse-like near-fault ground motions. Under certain conditions the near-fault ground motions could even result in smaller PA values than the case of MCE. This implies that the floor acceleration response is not very sensitive to velocity pulses of ground motion.

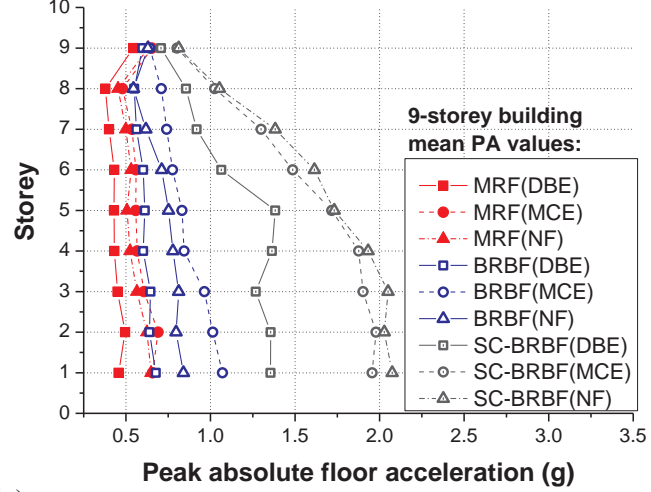
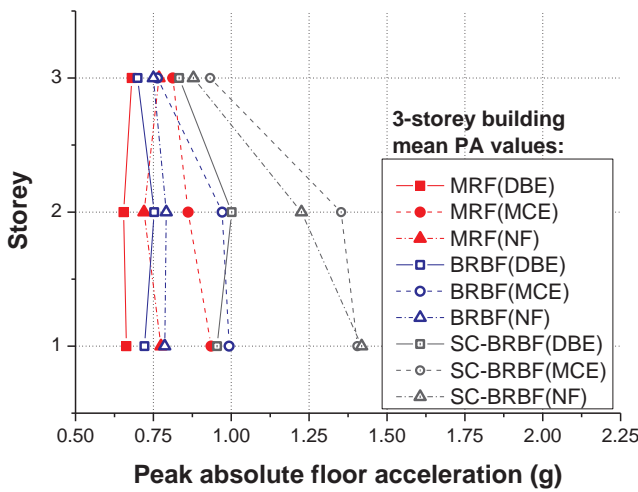
To enable a further understanding of the relationship between the structural responses and pulse characteristics of near-fault ground motions, the MID, RID, and PA responses of the three- and nine-storey buildings under each individual excitation are shown in Figs. 8 and 9. The mean, median and 84th percentile values of these key engineering demand quantities are provided, and some representative earthquakes (see Table 2 for event numbers) which cause relatively large responses are also marked in the figures. An evident dispersion of the results is generally shown, which is due to the uncertainty of the spectral characteristics of the near-fault ground motions. By examining the



(a)



(b)



(c)

Fig. 7. Mean seismic responses of structures to considered ground motions: (a) maximum inter-storey drift, (b) residual inter-storey drift, (c) peak absolute floor acceleration.

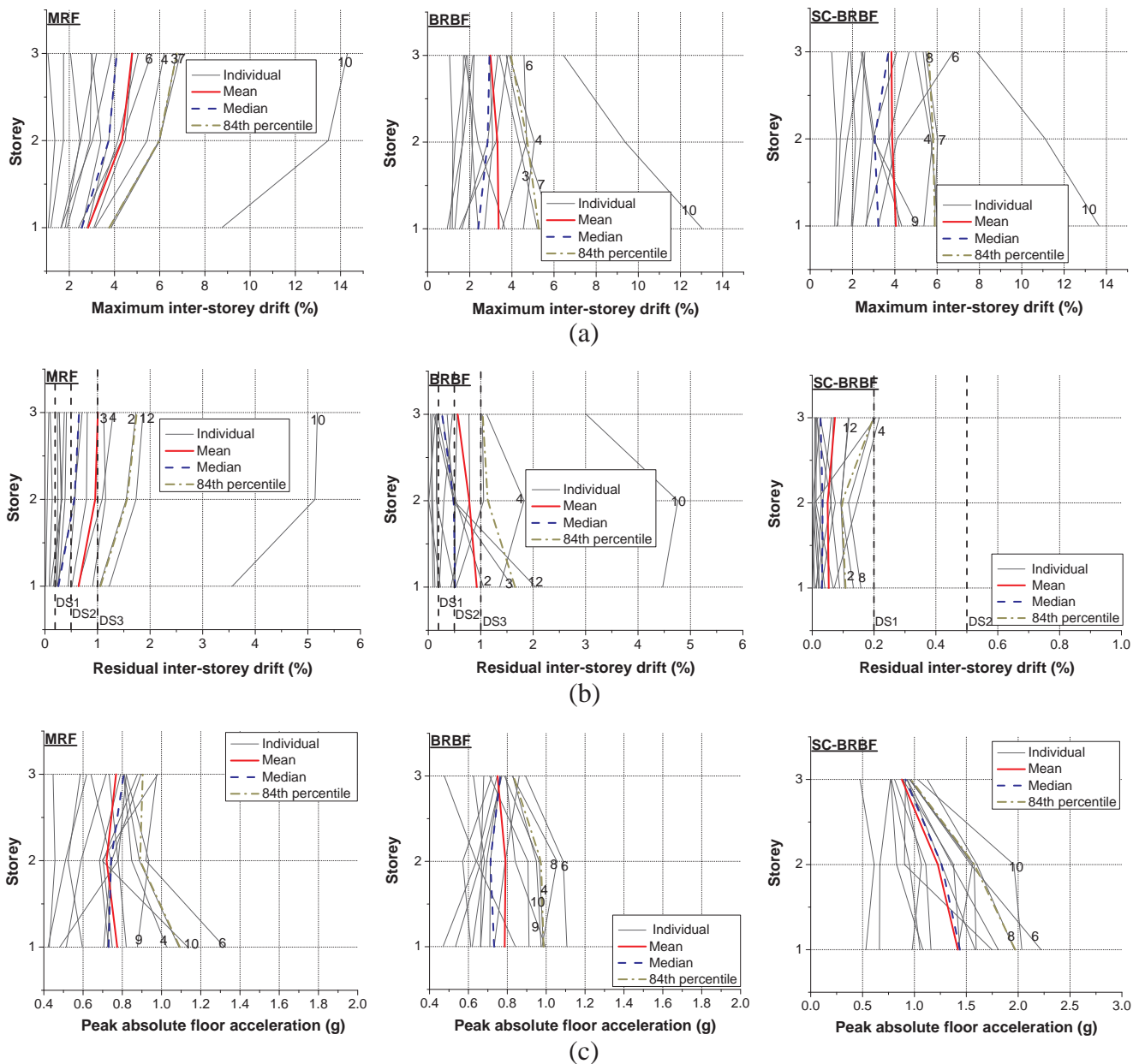


Fig. 8. Seismic responses of 3-storey buildings to individual near-fault ground motions: (a) maximum inter-storey drift, (b) residual inter-storey drift, (c) peak absolute floor acceleration.

individual responses, it is seen that the deformation responses are related to the spectral acceleration at the first mode period of the structure. Taking the three-storey braced frames for instance, relatively large MID and RID responses are obtained under ground motions NF2, NF4, NF6, NF8, and NF10. According to Fig. 5, these ground motions have relatively large spectral accelerations at approximately 0.64 s, i.e., the first mode period of the structure. Similarly, large deformation responses are generally obtained under ground motions NF2, NF3, NF9, and NF10 for the nine-storey braced frames, where these ground motions have relatively large spectral accelerations at approximately 1.73 s (the first mode period). It seems that there is a less clear correlation between the second mode period ($T_2 = 0.55$ s) and the deformation response of the nine-storey buildings. Although high-mode effect exists and could amplify the inter-storey drifts at certain floor levels, the maximum inter-storey drift (that among all the stories) is not critically influenced by the second mode period of vibration.

The PGV/PGA ratio, an indicator of the significance of the pulsing

effect, is found to be another factor that may affect the deformation responses of the structures. Taking the three-storey buildings for instance, ground motions NF2, NF6, NF8 generally have the largest first mode spectral accelerations, but the resulting MID and RID responses for the structures are much smaller than those induced by the Palos Verdes 2 earthquake (ground motion NF10). As can be seen from Table 2, the PGV/PGA ratio of the latter (0.303) is almost twice the value of the former (0.168 on average). In fact, the structures undergoing the Palos Verdes 2 (NF10) earthquake may have collapsed as the MID exceeds 10%. Similarly, for the nine-storey structures, the Elysian Park 3 (NF9) and Palos Verdes 2 (NF10) have the largest first mode spectral accelerations, but the peak deformation response to the former is significantly decreased due to the much lower PGV/PGA ratio (0.156 compared against 0.303). Pulse period can also affect the deformation responses of the structures. Although the two Chi-Chi ground motions (NF12 and NF15) have very large PGV/PGA ratios (more than 0.5), they generally cause noncritical deformation responses. This is probably

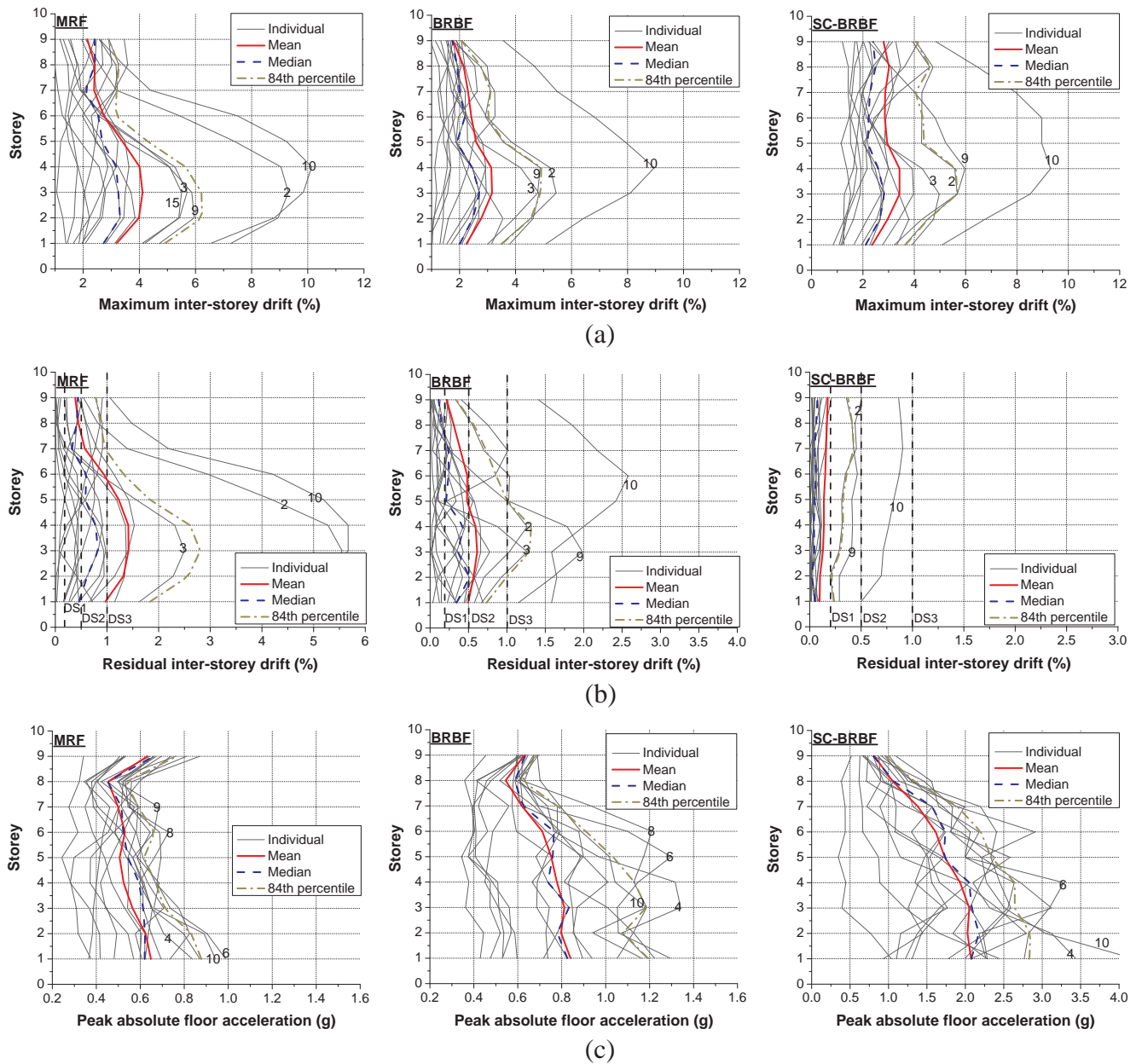


Fig. 9. Seismic responses of 9-storey buildings to individual near-fault ground motions: (a) maximum inter-storey drift, (b) residual inter-storey drift, (c) peak absolute floor acceleration.

because that the pulse periods (T_p or T_{p-v}) of the two ground motions far exceed the natural periods of the considered structures, causing no resonance with the velocity pulse. Furthermore, a certain correlation is found between the length-scale of the pulse (L_p) and the deformation demand. For instance, ground motion NF10, which leads to the largest deformation demand, has a relatively large L_p value. However, as the peak deformation response is a result of multiple factors, a larger L_p (e.g. NF12 and NF15) does not necessarily leads to a larger deformation demand.

The PA responses of the structures are not fully consistent with the deformation responses, although a large MID or RID is often accompanied by a large PA (e.g. ground motion NF10). Previous studies showed that the PA response is related to a large number of factors such number of stories, predominant period of vibration, mode shape, frequency content of ground motion, and extent of nonlinear behaviour of a building. In particular, it is generally perceived that a more pronounced nonlinear behaviour of the building often reduces floor

acceleration demands [62]. This may explain the inconsistency between the peak deformation and floor acceleration responses observed in the current study.

5. Further discussions

5.1. Parameter matrix

Following the discussion of the fundamental responses of the reference buildings to the considered far-field and near-fault earthquakes, the sensitivity of the braced frames to two important brace parameters, i.e., post-yield stiffness (α) and energy dissipation factor (β), are further investigated. The broadened parameter matrix covers three values of α , namely 0.01, 0.05 (reference case), and 0.1. A post-yield stiffness exceeding 0.1 is not considered in this study as this could cause overly high load resistance demands to the adjacent steel beams and columns. In addition, four levels of energy dissipation factor, i.e., $\beta = 0.5, 1.0,$

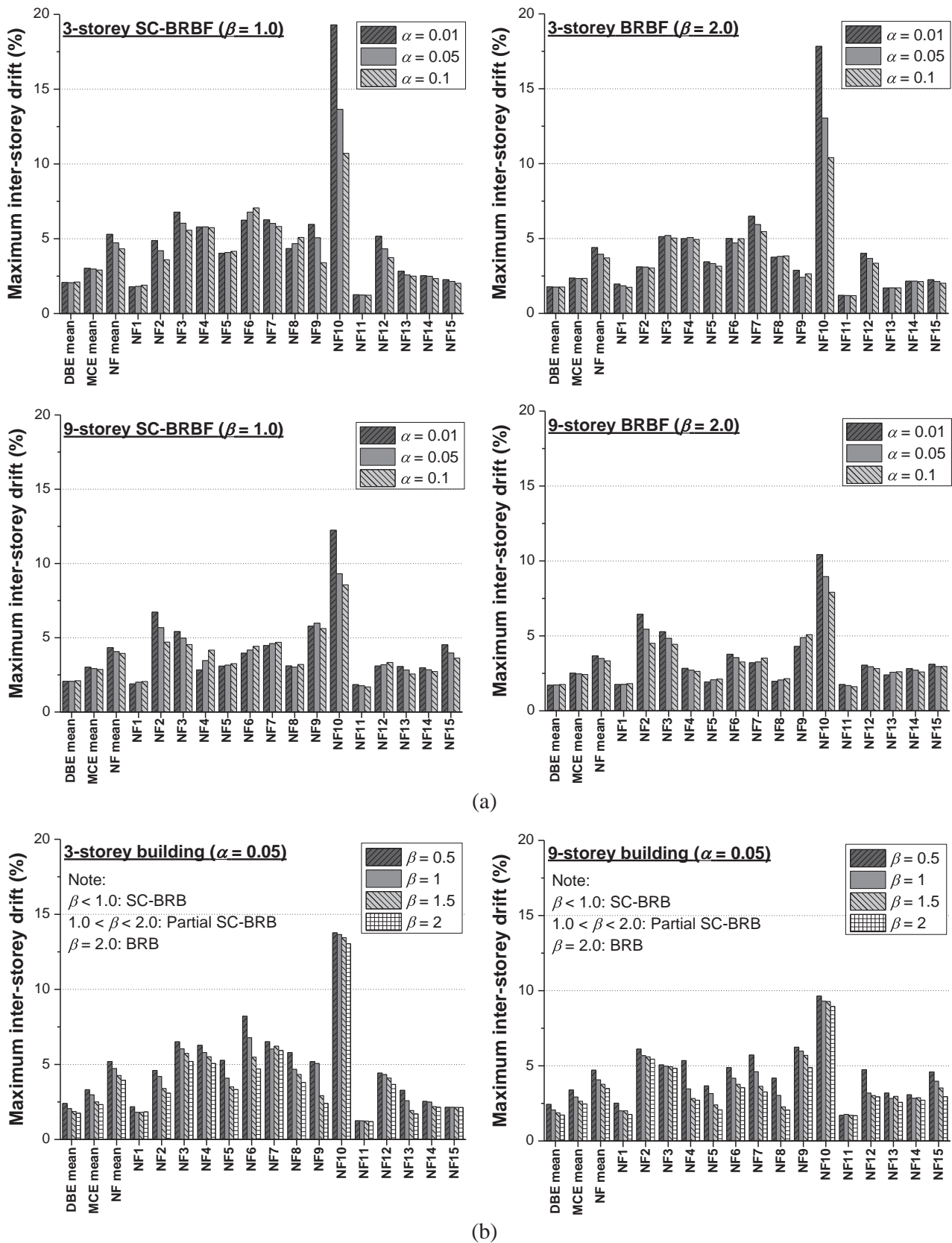


Fig. 10. Response of maximum inter-storey drift: (a) influence of α , (b) influence of β .

1.5, and 2.0, are considered. The case of $\beta = 0.5$ represents SC-BRBs with a reduced energy dissipation hysteresis but with a higher self-centring tendency, as compared with the reference case ($\beta = 1.0$). The case of $\beta = 1.5$ represents a typical partial SC-BRB where higher energy dissipation is provided but at the cost of compromised self-centring capability. The brace is deemed as an idealised BRB when $\beta = 2.0$. The same suites of the DBE/MCE far-field and the near-fault earthquakes are considered for the parametric study.

5.2. Parametric study results

Fig. 10 shows the mean MID responses of the braced frames with varying values of α and β to the far-field DBE/MCE as well as near-fault ground motions, together with the individual structural responses to each near-fault record. It is shown in Fig. 10(a) that for either the SC-BRBs or the BRBs under the far-field earthquakes, the post-yield stiffness has limited influence on the MID response. For the near-fault earthquakes, however, increasing the post-yield stiffness could slightly decrease the MID. A possible explanation is that an increase in α could mitigate storey drift concentration (weak storey) at large structural deformation, especially when the P- Δ effect is significant. As the pulse-like near-fault earthquakes lead to larger MID demands, the beneficial influence of the increased α in alleviating weak storey becomes noticeable. The results in Fig. 10(b) confirm that increasing β could indeed decrease the MID response to both the far-field and near-fault earthquakes. As mentioned before, this is attributed to the increased energy dissipation. It is of interest to find that compared with the tendency when β increases from lower values to 1.5, the decrease in MID when β increases from 1.5 to 2.0 is less remarkable. This suggests that partial SC-BRBs could lead to MID demands close to BRBs.

Fig. 11 gives the maximum RID responses of the considered structures. It is seen from Fig. 11(a) that increasing α always decreases the RID response for the BRBs, and such tendency is particularly remarkable under near-fault earthquakes. This phenomenon is related to the concept of “probabilistic self-centring” or “dynamic stability” which specifies that the actual RID is often smaller than the maximum possible RID computed as the one achieved after load is slowly removed from the MID [63]; the RID is reduced with increase in the probability that the structure undergoes inelastic deformations in the direction toward zero displacement rather than being away from zero displacement. Increasing the post-yield stiffness has been found to increase such probability, and hence decreasing the RID [64]. For the SC-BRBs, the post-yield stiffness has a much less significant influence on the RID response where the absolute RID has already been reduced to very small values. On the other hand, Fig. 11(b) clearly demonstrates that an increase in β significantly increases the RID, and such trend is especially obvious under the near-fault earthquakes. For either the three- or nine-storey buildings subjected to the near-fault earthquakes, decreasing β from 2.0 to 1.5 could effectively reduce the mean RID from around 1.0% (class DS3-DS4, according to FEMA P-58 [59]) to the 0.5% limit (class DS2). This suggests that a partial SC-BRB with $\beta = 1.5$ can be adequately effective in ensuring economically feasible repairs for structures after strong pulse-like excitations.

Regarding non-structural performances, as shown in Fig. 12, the PAs of the SC-BRBs and BRBs are not sensitive to the post-yield stiffness of the braces, but can be evidently influenced by the energy dissipation factor. The results suggest that the flag-shaped SC-BRBs with $\beta \leq 1.0$ are not desirable from the floor acceleration control point of view. This is due to the more abrupt transitions of the braces during the unloading and reloading path with a decrease in β , as mentioned before. An important finding is that the PA is remarkably suppressed when β increases from 1.0 to 1.5, whereas a further increase in β makes little further improvement. Based on the results given in Figs. 10–12, the partial SC-BRBs exhibit a good balance among the MID, RID, and PA responses for the steel braced frames. Although the PA is also effectively controlled when β increases to 2.0, unwanted larger RIDs are induced.

It is also found that the increase in β is more effective in controlling PA for the case of near-fault earthquakes than far-field ones.

5.3. RID prediction model

RID is an important parameter for judging the post-earthquake safety of a building and the economic feasibility of repair. For performance-based design, engineers may be interested in understanding the relationship between the MID and RID. Such relationship is particularly useful when a permissible RID level (e.g. 0.5%) is set and based on which a target MID level is to be determined. Alternatively, engineers can quickly estimate the RID and understand the resilience class of the designed structure based on the calculated MID. Theoretically speaking, the maximum possible RID cannot exceed the MID minus the elastic inter-storey drift. Due to “probabilistic self-centring”, as aforementioned, the actual RID is often less than the maximum possible static value. A normalised RID (i.e., RID_N), as expressed by Eq. (1), could be a simple index used to depict the relationship between RID and MID:

$$RID_N = \frac{\Delta_r}{\Delta_{\max} - \Delta_{el}} \quad (1)$$

where Δ_r is the maximum residual inter-storey drift of a structure among all the floors, Δ_{\max} is the maximum transient inter-storey drift of the structure, and Δ_{el} is the elastic inter-storey drift which, for ease of design, may be taken as the mean value for different stories or based on the roof drift pushover response. $\Delta_{\max} - \Delta_{el}$ is an upper bound for the amount of RID, and therefore RID_N ranges between 0.0 and 1.0.

Fig. 13 shows the mean RID_N of the considered buildings with varying α and β values under the far-field DBE/MCE and near-fault earthquakes. The mean RID_N generally falls within the range between 0.1 and 0.4, and it increases evidently with an increase in β , especially when $\beta \geq 1.0$. The difference in RID_N between the cases of $\beta = 0.5$ and $\beta = 1.0$ is not remarkable due to small residual drifts caused by the SC-BRBs. An increase in α also tends to decrease RID_N , and this trend is more obvious when the structures are subjected to near-fault earthquakes. The DBE and MCE seem to result in similar RID_N , but the near-fault ground motions result in larger RID_N values. This implies that the normalised RID is insensitive to the scale of the ground motion, but is more evidently influenced by the velocity pulses.

According to the current results, a curve fitting technique is used to facilitate performance-based design. Considering the fact that the energy dissipation factor β has the most evident influence on RID_N , quadratic polynomials in terms of β are found to adequately capture these trends, and the general form can be written as:

$$RID_N = A\beta^2 + B\beta + C \quad (2)$$

where A, B, and C are constants which vary with different cases and are obtained via least square regression, as summarised in Table 3. Designers may use the simple RID prediction model to quickly evaluate the relationship between RID and MID, at least for preliminary design stages. Although the current constants of the prediction model are derived based on particular cases, interpolated values may be used for parameters that fall within the considered ranges, depending on the designer's judgement.

6. Summary and conclusions

This paper has focused on the overall dynamic behaviour of MRFs, BRBs, and SC-BRBs under pulse-like near-fault earthquakes. The structural responses to far-field DBE- and MCE-level ground motions were also studied for comparison purpose. A set of carefully designed prototype buildings were analysed, and key engineering demand parameters such as MID, RID, and PA, were investigated in detail. A further parametric study was carried out, enabling a better understanding of the influences of varying brace characteristics on the responses of the braced frames. A RID prediction model was finally

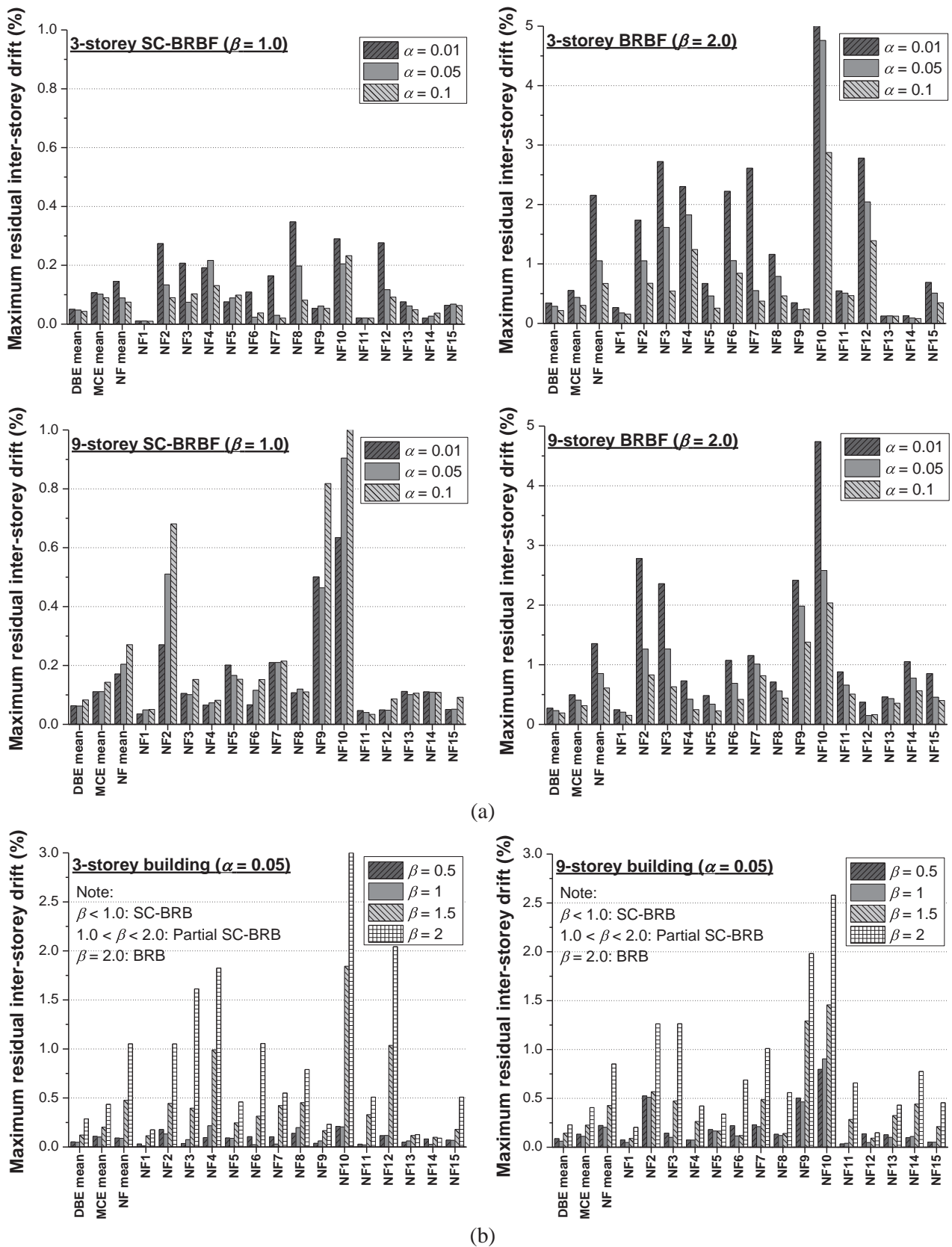


Fig. 11. Response of maximum residual inter-storey drift: (a) influence of α , (b) influence of β .

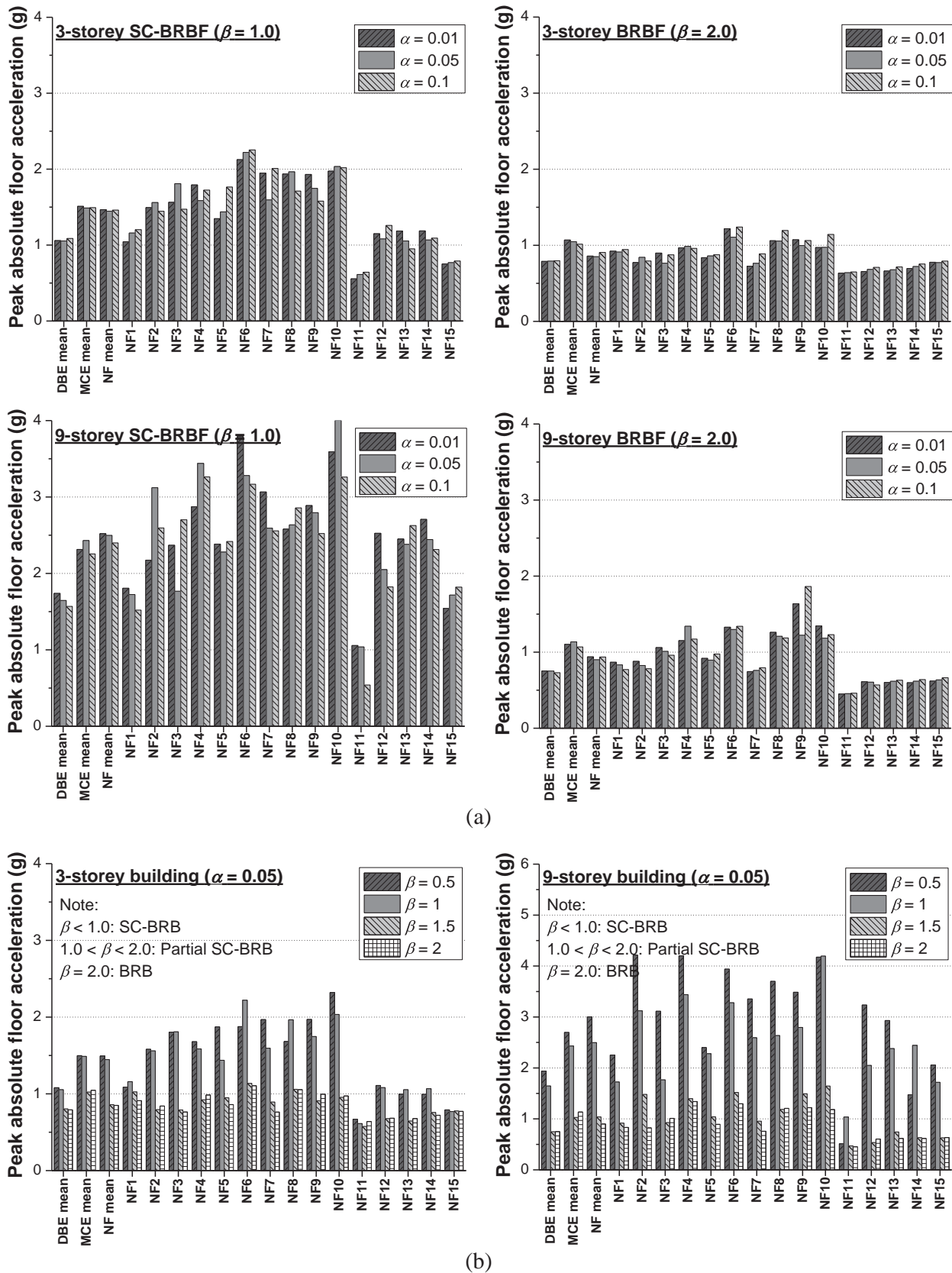


Fig. 12. Response of peak absolute floor acceleration: (a) influence of α , (b) influence of β .

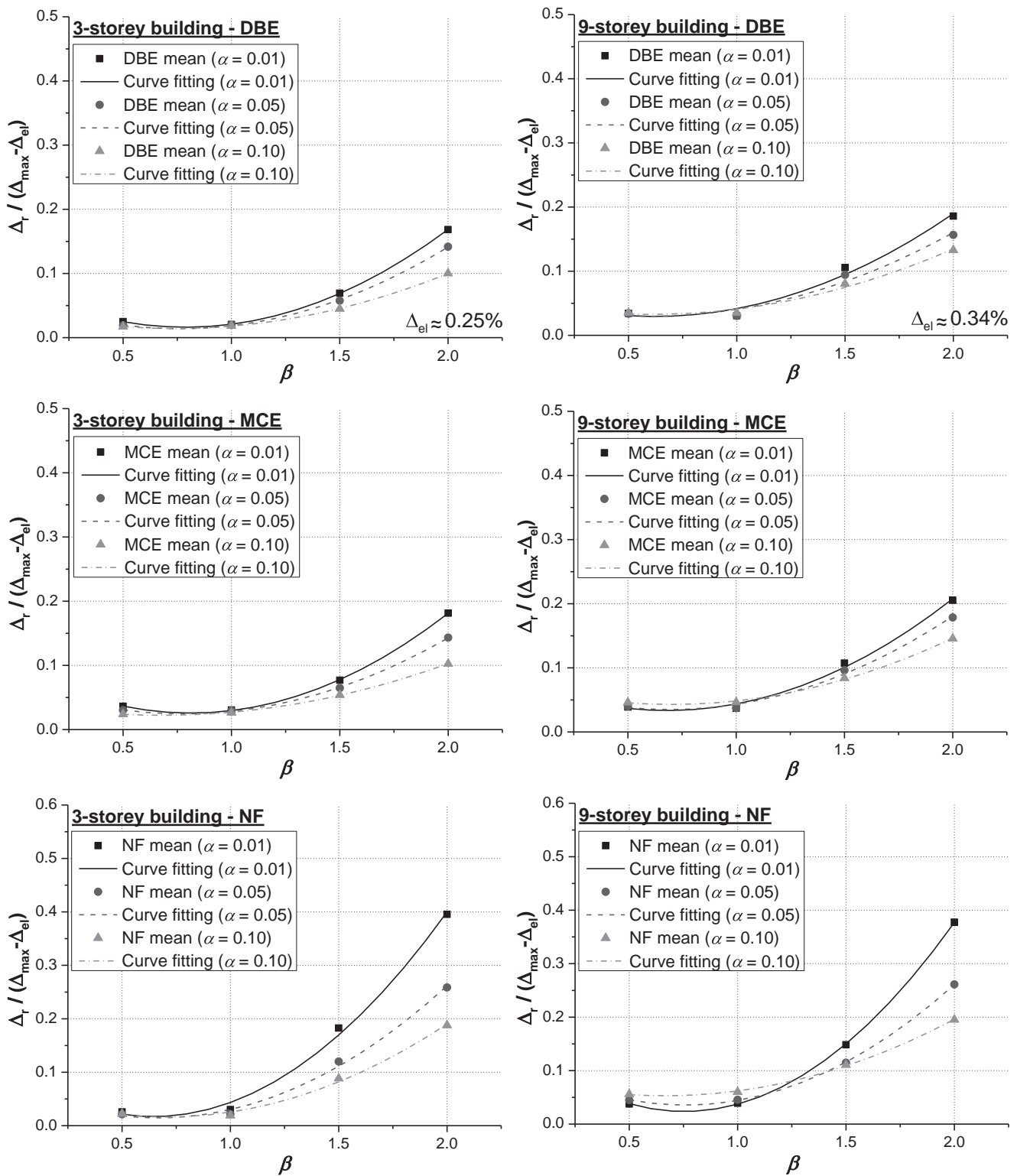


Fig. 13. Relationships between residual and maximum inter-storey drifts.

proposed to facilitate performance-based design. The key findings and conclusions are noted as follows.

- For all the considered steel frames, the near-fault earthquakes lead to significantly larger deformation demands than the DBE and MCE. The structural responses under the near-fault earthquakes are related to spectral accelerations and PGV/PGA ratios; in addition, larger deformation responses are more likely to occur when the

structural natural period is close to the pulse period of the ground motion.

- The MRFs and SC-BRBFs sometimes have comparable MID levels. The BRBFs tend to exhibit lower MID responses than the other two structural types. The decreased MID could be related to the high energy dissipation capability and high initial stiffness of the BRBs.
- Post-yield stiffness has a limited influence on the MID responses of the braced frames under the far-field earthquakes, but under the

Table 3
Constants for RID prediction model.

Case	Stiffness ratio	A	B	C
3-Storey-DBE	$\alpha = 0.01$	0.104	-0.164	0.081
	$\alpha = 0.05$	0.083	-0.127	0.062
	$\alpha = 0.10$	0.054	-0.080	0.044
3-Storey-MCE	$\alpha = 0.01$	0.110	-0.180	0.099
	$\alpha = 0.05$	0.079	-0.123	0.072
	$\alpha = 0.10$	0.046	-0.063	0.044
3-Storey-NF	$\alpha = 0.01$	0.208	-0.268	0.103
	$\alpha = 0.05$	0.138	-0.184	0.076
	$\alpha = 0.10$	0.103	-0.144	0.067
9-Storey-DBE	$\alpha = 0.01$	0.084	-0.104	0.061
	$\alpha = 0.05$	0.066	-0.078	0.053
	$\alpha = 0.10$	0.052	-0.063	0.052
9-Storey-MCE	$\alpha = 0.01$	0.100	-0.136	0.080
	$\alpha = 0.05$	0.085	-0.118	0.076
	$\alpha = 0.10$	0.061	-0.086	0.073
9-Storey-NF	$\alpha = 0.01$	0.228	-0.344	0.153
	$\alpha = 0.05$	0.146	-0.221	0.119
	$\alpha = 0.10$	0.080	-0.107	0.088

near-fault earthquakes, increasing the post-yield stiffness could help decrease the MID response. Increasing the energy dissipation factor is effective in decreasing the MID response.

- The SC-BRBFs generally have mean residual drifts less than 0.2% under all the considered ground motion records. For the MRFs/BRBFs under the DBE and MCE, the mean RIDs are below 0.3% and 0.5%, respectively. The near-fault ground motions lead to significantly increased RIDs for the MRFs/BRBFs, where the value could exceed 1.0%, suggesting that these structures may not be economically repairable under the considered near-fault earthquakes.
- The post-yield stiffness does not have a significant influence on the RID responses of SC-BRBFs. A decrease in energy dissipation factor significantly decreases the RID, and such tendency is particularly remarkable under near-fault earthquakes.
- The SC-BRBFs generally show much higher PA responses compared with the MRFs and BRBFs under all the considered ground motions. Pulse-like near-fault ground motions do not necessarily induce larger PA values than the far-field earthquakes.
- The PAs of the SC-BRBFs and BRBFs are not sensitive to the post-yield stiffness of the braces, but can be evidently influenced by the energy dissipation factor. Partial SC-BRBFs (e.g., $\beta = 1.5$) appear to be a desirable option that effectively controls the PA and RID responses without causing much larger MIDs than BRBFs. In other words, a good balance among the MID, RID, and PA responses can be achieved when partial SC-BRBFs are used.
- To facilitate performance-based design, RID prediction models were proposed which enable a quick evaluation of the relationship between MID and RID.

Acknowledgements

The financial supports from the National Natural Science Foundation of China (NSFC) with Grant Nos. 51778456, 51778459, 51820105013 are gratefully acknowledged. Supports for this study were also provided by International Joint Research Laboratory of Earthquake Engineering and Central University Fund for Interdisciplinary Research, Tongji University.

References

- [1] Nip KH, Gardner L, Elghazouli AY. Cyclic testing and numerical modelling of carbon steel and stainless steel tubular bracing members. *Eng Struct* 2010;32(2):424–41.
- [2] Tremblay R, Bolduc P, Neville R, DeVall R. Seismic testing and performance of buckling-restrained bracing systems. *Can J Civil Eng* 2006;33:183–98.
- [3] Fahnestock LA, Sause R, Ricles JM. Experimental evaluation of a large-scale buckling-restrained braced frame. *J Struct Eng* 2007;133(9):1205–14.
- [4] Chou CC, Chen SY. Subassemblage tests and finite element analyses of sandwiched buckling-restrained braces. *Eng Struct* 2010;32:2108–21.
- [5] Takeuchi T, Hajjar JF, Matsui R, Nishimoto K, Aiken ID. Local buckling restraint condition for core plates in buckling restrained braces. *J Construct Steel Res* 2010;66(2):139–49.
- [6] McCormick J, Aburano H, Ikenaga M, Nakashima M. Permissible residual deformation levels for building structures considering both safety and human elements. *Proc 14th world conf earthquake engineering*. Beijing: Seismological Press of China; 2008.
- [7] Sabelli R, Mahin S, Chang C. Seismic demands on steel braced frame buildings with buckling restrained braces. *Eng. Struct* 2003;25(5):655–66.
- [8] Pettinga D, Christopoulos C, Pampanin S, Priestley N. Effectiveness of simple approaches in mitigating residual deformations in buildings. *Earthq Eng Struct Dyn* 2007;36(12):1763–83.
- [9] Fahnestock LA, Sause R, Ricles JM. Seismic response and performance of buckling-restrained braced frames. *J Struct Eng* 2007;133(9):1195–204.
- [10] Erochko J, Christopoulos C, Tremblay R, Choi H. Residual drift response of SMRFs and BRB frames in steel buildings designed according to ASCE 7–05. *J Struct Eng* 2011;137(5):589–99.
- [11] Li Z, He M, Wang K. Hysteretic performance of self-centering glulam beam-to-column connections. *J Struct Eng* 2018;144(5):04018031.
- [12] Christopoulos C, Tremblay R, Kim HJ, Lacerte M. Self-centering energy dissipative bracing system for the seismic resistance of structures: development and validation. *J Struct Eng* 2008;134(1):96–107.
- [13] Chou CC, Chen YC, Pham DH, Truong VM. Steel braced frames with dual-core SCBs and sandwiched BRBs: mechanics, modeling and seismic demands. *Eng Struct* 2014;72:26–40.
- [14] Chou CC, Wu TH, Beato ARO, Chung PT, Chen YC. Seismic design and tests of a full-scale one-story one-bay steel frame with a dual-core self-centering brace. *Eng Struct* 2016;111:435–50.
- [15] Zhou Z, Xie Q, Lei XC, He XT, Meng SP. Experimental investigation of the hysteretic performance of dual-tube self-centering buckling-restrained braces with composite tendons. *J Compos Constr* 2015;19(6):04015011.
- [16] Wang W, Fang C, Liu J. Large size superelastic SMA bars: heat treatment strategy, mechanical property and seismic application. *Smart Mater Struct* 2016;25(7):075001.
- [17] Fang C, Zhou XY, Osofero AI, Shu Z, Corradi M. Superelastic SMA Belleville washers for seismic resisting applications: experimental study and modelling strategy. *Smart Mater Struct* 2016;25:105013.
- [18] Fang C, Yam MCH, Lam ACC, Zhang YY. Feasibility study of shape memory alloy ring spring systems for self-centring seismic resisting devices. *Smart Mater Struct* 2015;24:075024.
- [19] Miller DJ, Fahnestock LA, Eatherton MR. Development and experimental validation of a nickel-titanium shape memory alloy self-centering buckling-restrained brace. *Eng Struct* 2012;40:288–98.
- [20] Qiu C, Zhu S. Shake table test and numerical study of self-centering steel frame with SMA braces. *Earthq Eng Struct Dyn* 2017;46(1):117–37.
- [21] Fang C, Yam MCH, Lam ACC, Xie LK. Cyclic performance of extended end-plate connections equipped with shape memory alloy bolts. *J Constr Steel Res* 2014;94(94):122–36.
- [22] Fang C, Yam MCH, Ma HW, Chung KF. Tests on superelastic Ni-Ti SMA bars under cyclic tension and direct-shear: towards practical recentering connections. *Mater Struct* 2013;48(4):1013–30.
- [23] Yam MCH, Fang C, Lam ACC, Zhang YY. Numerical study and practical design of beam-to-column connections with shape memory alloys. *J Constr Steel Res* 2015;104:177–92.
- [24] Wang W, Fang C, Liu J. Self-centering beam-to-column connections with combined superelastic SMA bolts and steel angles. *J Struct Eng* 2017;143(2):04016175.
- [25] Fang C, Wang W, He C, Chen YY. Self-centring behaviour of steel and steel-concrete composite connections equipped with NiTi SMA bolts. *Eng Struct* 2017;150:390–408.
- [26] Moradi S, Alam MS, Asgarian B. Incremental dynamic analysis of steel frames equipped with NiTi shape memory alloy braces. *Struct Des Tall Spec Build* 2014;23:1406–25.
- [27] Kari A, Ghassemieh M, Abolmaali SA. A new dual bracing system for improving the seismic behavior of steel structures. *Smart Mater Struct* 2011;20:125020.
- [28] Eatherton MR, Fahnestock LA, Miller DJ. Computational study of self-centering buckling-restrained braced frame seismic performance. *Earthq Eng Struct Dyn* 2014;43:1897–914.
- [29] Qiu CX, Zhu S. High-mode effects on seismic performance of multi-story self-centering braced steel frames. *J Constr Steel Res* 2016;119:133–43.
- [30] Alavi B, Krawinkler H. Strengthening of moment-resisting frame structures against near-fault ground motion effects. *Earthq Eng Struct Dyn* 2004;33(6):707–22.
- [31] Gerami M, Abdollahzadeh D. Vulnerability of steel moment-resisting frames under effects of forward directivity. *Struct Des Tall Special Build* 2015;24(2):97–122.
- [32] Yadav KK, Gupta VK. Near-fault fling-step ground motions: characteristics and simulation. *Soil Dyn Earthq Eng* 2017;101:90–104.
- [33] Makris N, Psychogios T. Dimensional response analysis of yielding structures with first-mode dominated response. *Earthq Eng Struct Dyn* 2006;35(10):1203–24.
- [34] Dimakopoulou V, Fragiadakis M, Spyarakos C. Influence of modeling parameters on the response of degrading systems to near-field ground motions. *Eng Struct* 2013;53(8):10–24.

- [35] Karavasilis TL, Makris N, Bazeos N, Beskos DE. Dimensional response analysis of multistory regular steel MRF subjected to pulse-like earthquake ground motions. *J Struct Eng* 2010;136(8):921–32.
- [36] Alonso-Rodríguez A, Miranda E. Assessment of building behavior under near-fault pulse-like ground motions through simplified models. *Soil Dyn Earthq Eng* 2015;79:47–58.
- [37] Dicleli M, Mehta A. Effect of near-fault ground motion and damper characteristics on the seismic performance of chevron braced steel frames. *Earthq Eng Struct Dyn* 2007;36(7):927–48.
- [38] Ruiz-García J, Negrete-Manriquez JC. Evaluation of drift demands in existing steel frames under as-recorded far-field and near-fault mainshock–aftershock seismic sequences. *Eng Struct* 2011;33(2):621–34.
- [39] Ismail M, Rodellar J, Pozo F. An isolation device for near-fault ground motions. *Struct Contr Health Monit* 2014;21(3):249–68.
- [40] Mazza F, Mazza M, Vulcano A. Base-isolation systems for the seismic retrofitting of r.c. framed buildings with soft-storey subjected to near-fault earthquakes. *Soil Dyn Earthq Eng* 2018;109:209–21.
- [41] Tzimas AS, Kamaris GS, Karavasilis TL, Galasso C. Collapse risk and residual drift performance of steel buildings using post-tensioned MRFs and viscous dampers in near-fault regions. *Bull Earthq Eng* 2016;14(6):1643–62.
- [42] Vafaei D, Eskandari R. Seismic performance of steel mega braced frames equipped with shape-memory alloy braces under near-fault earthquakes. *Struct Des Tall Special Build* 2016;25(1):3–21.
- [43] Tremblay R, Lacerte M, Christopoulos C. Seismic response of multistory buildings with self-centering energy dissipative steel braces. *J Struct Eng* 2008;134(1):108–20.
- [44] Gupta A, Krawinkler H. Seismic demands for performance evaluation of steel moment resisting frame structures (SAC Task 5.4.3) Report No 132 CA: John A. Blume Earthquake Engineering Center, Stanford University; 1999.
- [45] American Society of Civil Engineers (ASCE). Minimum design loads for buildings and other structures. Reston, VA: ASCE/SEI 7-10; 2010.
- [46] Wang W, Fang C, Yang X, Chen YY, Ricles J, Sause R. Innovative use of a shape memory alloy ring spring system for self-centering connections. *Eng Struct* 2017;153:503–15.
- [47] Silwal B, Ozbulut OE, Michael RJ. Seismic collapse evaluation of steel moment resisting frames with superelastic viscous damper. *J Constr Steel Res* 2016;126:26–36.
- [48] Mazzoni S, McKenna F, Scott M, Fenves G. Open system for earthquake engineering simulation (OpenSees). Berkeley: User command language manual, Pacific Earthquake Engineering Research Center, University of California; 2006.
- [49] Federal Emergency Management Agency (FEMA). Quantification of building seismic performance factors. FEMA P695; 2009.
- [50] Bray JD, Rodriguez-Marek A. Characterization of forward-directivity ground motions in the near-fault region. *Soil Dyn Earthq Eng* 2004;24:815–28.
- [51] Loh CH, Wan S, Liao WI. Effects of hysteretic model on seismic demands: consideration of near-fault ground motions. *Struct Des Tall Build* 2002;11:155–69.
- [52] Krawinkler H, Alavi B. Development of improved design procedures for near-fault ground motions. SMIP 98, Seminar on utilization of strong motion data, Oakland, CA. 1998.
- [53] Rodriguez-Marek A. Near-fault seismic site response PhD Dissertation University of California at Berkeley; 2000
- [54] Mavroeidis GP, Papageorgiou AS. A mathematical representation of near-fault ground motions. *Bull Seismol Soc Am* 2003;93(3):1099–131.
- [55] Somerville Paul G. Magnitude scaling of the near fault rupture directivity pulse. *Phys Earth Planet Inter* 2003;137:201–12.
- [56] Priestley MJN. Myths and fallacies in earthquake engineering – Conflicts between design and reality. *Bull New Zealand Nat Soc Earthq* 1993;26(3):329–41.
- [57] Christopoulos C, Filiatrault A, Folz B. Seismic response of self-centering hysteretic SDOF systems. *Earthq Eng Struct Dyn* 2002;31:1131–50.
- [58] Kazantzi AK, Vamvatsikos D. The hysteretic energy as a performance measure in analytical studies. *Earthq Spectra* 2018;34(2):719–39.
- [59] Federal Emergency Management Agency (FEMA). Seismic performance assessment of buildings. Methodology vol. 1. FEMA P-58-1; 2012.
- [60] Shu Z, Zhang J, Nagarajaiah S. Dimensional analysis of inelastic structures with negative stiffness and supplemental damping devices. *J Struct Eng* 2016;143(3):04016184.
- [61] Karavasilis TL, Seo CY. Seismic structural and non-structural performance evaluation of highly damped self-centering and conventional systems. *Eng Struct* 2011;33(8):2248–58.
- [62] Ray-Chaudhuri S, Hutchinson TC. Effect of nonlinearity of frame buildings on peak horizontal floor acceleration. *J Earthq Eng* 2011;15(1):124–42.
- [63] MacRae GA, Kawashima K. Post-earthquake residual displacements of bilinear oscillators. *Earthq Eng Struct Dyn* 1997;26:701–16.
- [64] Eatherton MR, Hajjar JF. Residual drifts of self-centering systems including effects of ambient building resistance. *Earthq Spectra* 2011;27(3):719–44.